Consistent seismic hazard and fragility analysis considering combined capacity-demand uncertainties via probability density evolution method

Article *in* Structural Safety · April 2023

3 authors, including:

Xu-Yang Cao
Hohai University

De-Cheng Feng
Southeast University

Consistent seismic hazard and fragility analysis considering combined capacity-demand uncertainties via probability density evolution method

Xu-Yang Cao[a], De-Cheng Feng[b,*], Michael Beer[c,d,e]

[a] *College of Civil and Transportation Engineering, Hohai University, Nanjing 210098, China*
[b] *Key Laboratory of Concrete and Prestressed Concrete Structures of the Ministry of Education, Southeast University, Nanjing 210096, China*
[c] *Institute for Risk and Reliability, Leibniz University Hannover, Callinstr. 34, Hannover, Germany*
[d] *Institute for Risk and Uncertainty, University of Liverpool, Peach Street, L69 7ZF Liverpool, United Kingdom*
[e] *International Joint Research Center for Engineering Reliability and Stochastic Mechanics, Tongji University, Shanghai 200092, China*

Abstract

A consistent seismic hazard and fragility framework considering combined capacity-demand uncertainties is proposed, in light of the probability density evolution method (PDEM). The PDEM has solid theoretical basis in the reliability field, and it is integrated within the performance-based earthquake engineering (PBEE) for hazard-fragility assessment in this paper. During the analysis, the sample sets with different assigned probability are required to determine in advance, and the equivalent extreme events with virtual stochastic process are required to establish for solution. Both the uncertainties of capacity and demand are considered, and a combined performance index (CPI) is defined as concerned physical variable in PDEM, through pushover static and timehistory dynamic analyses. A non-stationary stochastic earthquake model is introduced using spectral representation of random functions, and the real characteristics of ground motions are reflected by one or two variables for each probability space. The peak ground acceleration (PGA) and spectral acceleration of the first period [$S_a(T_1)$] of non-stationary stochastic ground motions are then obtained for each earthquake level, and the equivalent extreme events are also performed to discuss the statistical information of PGA or $S_a(T_1)$ through PDEM. The exceeding probability of PGA or $S_a(T_1)$ for each earthquake level is acquired, and a connection between the fragility value and hazard extent is built. The final 3D consistent hazard-fragility curves are then given, and the exceeding probability for different limit states, earthquake levels as well as intensity exceeding conditions can be predicted. Moreover, a comparison with the four classic approaches in the state-of-the-art is performed to verify the accuracy of PDEM procedure. In general, the framework avoids the pre-defined lognormal fragility shape and proves the combined efficiency and accuracy with the Monte Carlo simulation (MCS). The consistency from probabilistic hazard to fragility is realized without re-selecting earthquake waves, which is mainly attributed to the application of PDEM and non-stationary ground motions. The proposed framework provides new ideas for the consistent non-parametric hazard and fragility assessment scheme in the PBEE.

Keywords: Probabilistic performance, Seismic fragility, Seismic hazard, Stochastic earthquake, Structural assessment, PDEM

1. Introduction

With the development of performance-based earthquake engineering (PBEE) in seismic community in recent decades, researchers are focusing more on the service-period capacity and life-cycle maintenance of

*Corresponding author.
Email addresses: caoxy@hhu.edu.cn (Xu-Yang Cao), dcfeng@seu.edu.cn (De-Cheng Feng), beer@irz.uni-hannover.de (Michael Beer)

engineering structures, more than the instantaneous structural behaviors. At this stage, the risk-based PBEE framework has received extensive attention, which obtains quantitative data of earthquake damage at various levels and other undesirable consequences based on the full probability theory. The risk-based PBEE framework was proposed by Cornel et al. [1], and the framework takes risk assessment as output, which is very important for strategy formulating before hazards and decision making after hazards, so as to reduce the earthquake losses of all parties [2, 3].

In the risk-based PBEE framework, the first step is the probabilistic seismic hazard analysis (PSHA), which refers to the evaluation of the probability level of different earthquake impacts that the engineering construction site may be subjected to in different years in the future [4]. The earthquake impacts can be generally expressed as intensity measures such as ground motion acceleration (PGA) and spectral acceleration of the first period [$S_a(T_1)$]. McGuire [5] reviewed the early history of PSHA and mentioned that it is the basis for seismic design of engineering structures from common buildings to critical facilities. Tothong et al. [6] extended the PSHA concept and incorporated the occurring possibility of velocity pulse in the near-fault earthquake. The disaggregation of PSHA explained the probability caused by pulse-like components and the conditional distribution associated with the pulse period. The research provided basis for appropriate earthquake selections in near-fault zones and improved the PSHA accuracy. Iervolino et al. [7] performed the aftershock PSHA to evalute the short-term risk management of structures, conditional to mainshock events. The combining results for mainshockaftershocks seismic sequences were also derived to realize a seismic hazard integral, which helped to evaluate the hazard occurrence rate of exceeding a specific limitation. Convertito and Herrero discussed [8] the seismic focal mechanism and source parameters in PSHA, and a theoretical corrective coefficient for different faulting types was analyzed through the attenuation law. The results concluded the significance of seismic strike-slip activity in hazaed assessment and compared with the regular faulting events through an application. In addition, Rahman et al. [9], Bhatti et al. [10], Ebrahimian et al. [11], Mahsuli et al. [12], Stirling et al. [13] performed the PSHA of different countries such as Bangladesh, Pakistan, Italy, Iran and New Zealand, and recommended the corresponding earthquake selection strategy in align with the country codes.

Although the current seismic hazard analyses can evaluate the earthquake intensities with different exceeding probabilities for a certain time period and specific site, a noteworthy issue during the process is the selection of ground motions and the uncertainty transmission from hazards to structures. Under the present probabilistic framework, the earthquakes adopted for PSHA generally differ from the earthquakes used for fragility analysis, which indicates that a re-selecting procedure of ground motions is commonly needed for structural dynamic analysis to acquire the performance index as well as to establish the seismic fragility curves. Therefore, the probability relationship from hazard to fragility is not consistent and it is difficult to directly meet the conditional probability in the full-probability formula of the risk-based PBEE framework. How to choose appropriate ground motions in seismic fragility analysis has become a long-term unresolved problem. With the development of stochastically generated ground motion in seismic risk assessment procedure, its applicability and superiority has been gradually recognized. Commonly, a stochastic earthquake model can characterize the stochastic process via a few variables and parameters, which critically incorporates the concerned factors and efficiently simplifies the excitation procedure. In this way, the stochastically generated ground motions can be well adopted into the PBEE framework for probabilistic evaluation. Jalayer and Beck [14] adopted seismic source parameters and proposed a stochastic earthquake model to realize the entire probabilistic time-history representation. Subset simulation was combined to derive small failure probabilities under different limit states, and the influence of two alternative representations of earthquake uncertainty was well compared via practical hazard cases. Rezaeian and Kiureghian [15] introduced a procedure of stochastically generated ground motions under specified site characteristics, and a parameterized stochastic model in light of white-noise process was well realized. A series of the s-tochastic model factors were ideally identified, including the fundamental frequency, acceleration bandwidth, and intensity tendency, which provided an important reference for the earthquake selections in probabilistic performance assessment. Gidaris et al. [16] utilized the stochastic ground motions and proposed an efficient probabilistic risk assessment framework. A kriging surrogate model was incorporated into the framework, and a benchmark four-story frame building was well applied to verify the efficiency of stochastic ground motions and the accuracy of risk assessment framework, which laid a significant basis for the subsequent researches.

Furthermore, the second step in the risk-based PBEE framework is the probabilistic seismic fragility analysis (PSFA), which refers to the evaluation in the probability of structural responses exceeding different limit states under the earthquake impacts [17]. This work quantitatively describes the seismic performance of engineering structures in a probabilistic sense, and reflects the relationship between the intensity of ground motion and the degree of structural damage from a macro perspective [18, 19]. The conventional empirical PSFA is established based on the previous seismic survey data and is generally used for performance evaluation of group buildings in a regional range. At this stage, the analytical PSFA is the mostly adopted approach, and a lognormal distribution assumption is commonly adopted for both structural capacity and demand. After performing a series of incremental dynamic analyses or multiple stripe analyses, the engineering demand parameters such as the maximum drift ratios are acquired, and the analytical fragilities are then generated through linear regression or maximum likelihood estimation. Lupoi et al. [20] evaluated the seismic fragility of realistic systems through nonlinear dynamic analyses and the probabilistic distributions of structural demands were analyzed. Two applications into concrete girders and buildings verified the efficiency of the method. Shinozuka et al. [21] established the analytical fragility procedure via the maximum likelihood estimation, and a lognormal distribution shape of the fragility model was analyzed with two parameters. The results were compared with the empirical fragility through history data, indicating an ideal matching degree. Schotanus et al. [22] developed a statistical approach for fragility estimation of time-changing systems, and a statistical model was proposed to judge the limit state function of structural capacity analytically. An application into three dimensional frames was carried out to verify the robustness of the approach. Choi et al. [23] discussed the seismic fragility of four typical bridges through synthetic earthquakes, and a first-order reliability principle was introduced to convert the individual components into entire structures. The vulnerability of bridges with different spans and types was compared and concluded. In addition, the PSFA into different structures and infrastructures were performed by researchers broadly, such as offshore wind turbine [24], unreinforced masonry structures [25], geostructures [26], concrete dams [27], external substructures [28], which predicted the tendency of structural performances under various earthquake levels and provided the basis for structural risk assessments in the probability perspective.

Worth noticing herein is that the current procedure in the PSFA is commonly based on the lognormal distribution assumption for variables, and this may be different with the accurate conditions. According to Ning [29], the lognormal distribution assumption for engineering demand parameter is idealized and is not applicable under a larger intensity condition. According to Karamlou et al. [30], the lognormal distribution assumption is lack of accuracy, especially for the real environment with strong material-geometric nonlinearity. Mangalathu and Jeon [31] also carried out relevant researches of seismic fragility and pointed out that the lognormal distribution assumption of variables can result in unrealistic predictions. Moreover, the accuracy of fragility results under the lognormal distribution assumption is mainly related to the number of samples. For instance, in the linear regression approach, the accuracy of fragility is affected by the slope and intercept of the regression relationship, and the values of the two parameters can be quite different for different sample number, thus the obtained fragility curve is still questionable. With the development of the non-parametric PSFA, a series of non-parametric strategies in failure probability characterization have been proposed by researchers, among which the probability density evolution method (PDEM) is an important subdivision. The PDEM has solid theoretical basis and verified mathematical derivations in the reliability field. It divides the sample space with different assigned probability, and summarizes the evolution tendency through numerical difference. The target variables with clear physical meanings are analyzed and the reliability trends with non-parametric characteristics are developed. Li et al. [32, 33] first proposed the PDEM theory and established the analyzing framework for nonlinear stochastic systems. Chen et al. [34, 35] developed the PDEM theory, and proposed the efficient point-selection approaches for different assigned-probability space with uncertain parameters. Moreover, Fan et al. [36] introduced a Bayesian updating approach for deteriorating engineering structures via PDEM, Wan et al. [37] performed the life-cycle reliability evaluation through combining PDEM and probability measure change, Zhou and Peng [38] adopted the active learning technique and enhanced the active subspace for high-dimensional reliability assessment of structures via PDEM, and Feng et al. [39] proposed an enhanced PDEM and reliability procedure incorporating multiple limit states and failure patterns. However, the strategy to establish the 3D consistent non-parametric seismic hazard-fragility framework via PDEM is not well researched at this stage, and the corresponding influence under the combined capacity-demand uncertainties via PDEM still requires further in-depth exploration.

Confronted with the above aspects, a consistent seismic hazard and fragility framework considering combined capacity-demand uncertainties is proposed in this paper, in light of the PDEM theory. The PDEM is integrated within the risk-based PBEE framework, and an equivalent extreme event with virtual stochastic process of PDEM is adopted for both PSHA and PSFA. Then a consistent three dimensional hazard-fragility relationship is established. During the process, a non-stationary stochastic earthquake model is introduced through spectral representation of random functions, and the real characteristics of ground motions are reflected by one or two variables for each probability space. The combined uncertainties of structural responses and limit states are considered for each probability space, with a combined performance index (CPI) expressed as demand minus capacity. Moreover, a comparison with the four classic approaches in the state-of-the-art is performed to verify the accuracy of PDEM procedure. In general, the framework avoids the pre-defined lognormal fragility shape and proves the combined efficiency and accuracy with the Monte Carlo simulation (MCS) [40]. Both the uncertainties of capacity, demand and earthquake are considered, and the consistency from probabilistic hazard to fragility is realized through the PDEM and non-stationary ground motions, which provides new ideas for the consistent non-parametric risk-based assessment scheme in the PBEE.

2. Consistent seismic hazard and fragility analysis via PDEM

In light of the risk-based PBEE framework with full probability theory [1], the uncertainty propagation from hazard to decision can be expressed as (Eq. 1):

$$\zeta(DV) = \int\int\int P(DV|DM) \cdot dP(DM|EDP) \cdot dP(EDP|IM) \cdot d\zeta(IM) \tag{1}$$

where IM is the intensity measure and denotes the hazard extent of earthquakes, EDP is the engineering demand parameter and denotes the concerned physical demand (D) of the structural system, DM is the damage measure and denotes the capacity level (C) of the structural system, DV is the decision variable and denotes the risk or loss of the integrated system. P[X|Y] represents the conditional probability of variable X under the limitation Y, and $\zeta(\cdot)$ denotes the exceeding frequency of the corresponding variable for a certain time period [41].

In Eq. 1, the section ζ(IM) is commonly regarded as PSHA and the section P(DM|EDP)·dP(EDP|IM) is commonly regarded as PSFA as follows (Eq. 2):

$$P(DM|IM) = \int P(DM|EDP) \cdot dP(EDP|IM) = P(D > C|IM) \tag{2}$$

The Eq. 2 constitutes the primary link in Eq. 1 and provides the basis for final decision making, which reflects the transmission of randomness from hazard to structure. To be specific, Eq. 2 means the seismic fragility with the exceeding probability of structural demand over structural capacity under a given earthquake level. The uncertainty of demand (resulting from ground motions) is commonly more intense than that of structural capacity, thus a great many researches of seismic fragility neglect the capacity uncertainty for simplification. According to Yu [42], capacity uncertainty may lead to obvious difference in calculation especially for new structural type, and adopting the deterministic thresholds as recommended in codes may underestimate the structural performance level. Thus, in this paper, both the uncertainties of demand and capacity are considered. The structural demand is obtained through time history analysis, and the structural capacity is obtained through pushover analysis. Then, a combined performance index (CPI) is introduced as demand minus capacity (D-C), and Eq. 2 can be transformed into (Eq. 3):

$$P(DM|IM) = P(D - C > 0|IM) = P(CPI > 0|IM) = 1 - P(CPI \leqslant 0|IM) \tag{3}$$

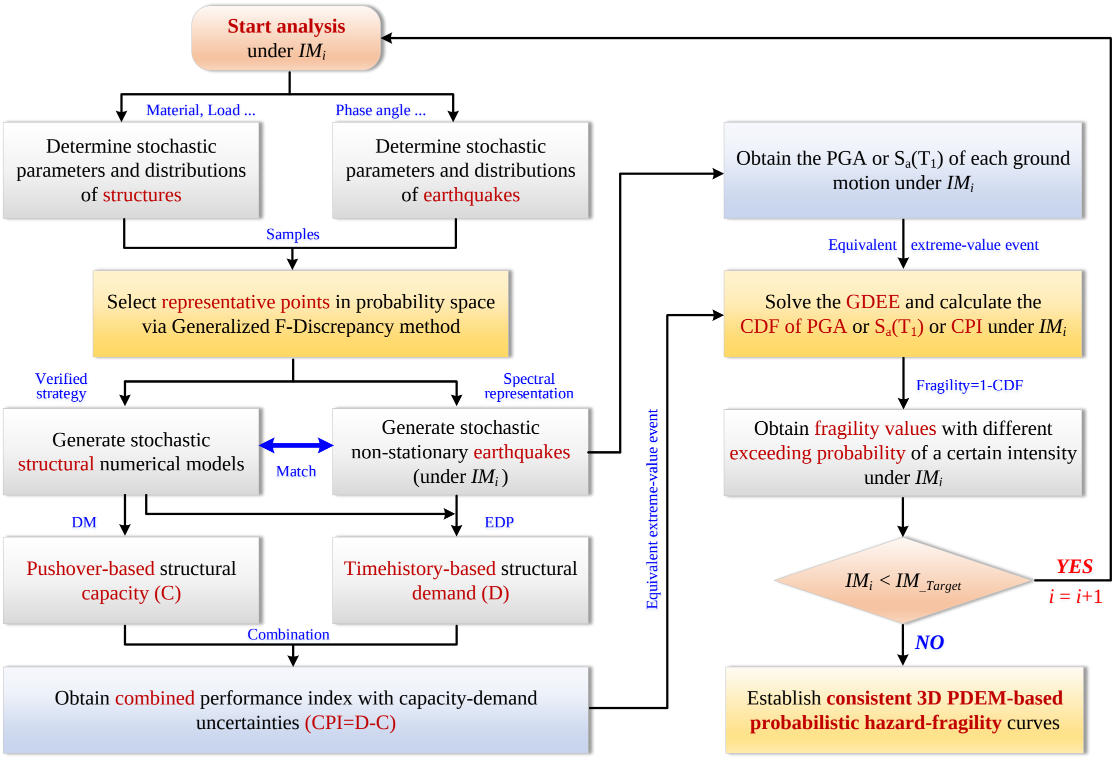

Figure 1: The flowchart of the consistent seismic hazard and fragility analysis via PDEM

The utilizations of combined demand-capacity functions as performance index are available in the literature and can be expressed in different versions. For instance, Jalayer et al. [43, 44] adopted the demand to capacity ratio to reflect its combined influence in structural dynamic behaviors and systematic fragility assessment, and their recent research provided a comprehensive description of the reason why the use of demand to capacity ratio as performance index is indeed critically beneficial [45]. More references related to this aspect can be found in Vamvatsikos and Cornell [46], Surahman [47], and Hernandez et al. [48]. According to the Eq. 3, the PSFA of a structural system is connected to the distribution of variable CPI under the earthquake level IM. More generally, for a variable X, P(X$\leqslant$0) indicates the value of cumulative distribution function (CDF) at the X=0, thus, Eq. 3 can be further re-written as (Eq. 4):

$$P(DM|IM) = 1 - CDF_{CPI|IM}(0) = 1 - \int_{-\infty}^{0} p_{CPI|IM} \tag{4}$$

where $p_{CPI|IM}$ denotes the probability density function (PDF) of variable CPI under the earthquake level IM. To better reflect the PDF of the concerned variable and avoids the pre-defined shape of the distribution type, the well-known probability density evolution method (PDEM) is then introduced, which has solid theoretical basis and verified mathematical derivations in the reliability field. Without the loss of generality, the dynamic-motion balance equation of a structural system under earthquake excitation can be presented as (Eq. 5):

$$\boldsymbol{M}\ddot{\boldsymbol{X}}(\boldsymbol{\Theta}, t) + \boldsymbol{C}\dot{\boldsymbol{X}}(\boldsymbol{\Theta}, t) + \boldsymbol{K}\boldsymbol{X}(\boldsymbol{\Theta}, t) = -\boldsymbol{M}\ddot{x}_g(\boldsymbol{\Theta},\ t) \tag{5}$$

where $\boldsymbol{M}$, $\boldsymbol{C}$ and $\boldsymbol{K}$ represent the $n \times n$ mass matrix, damping matrix and stiffness matrix of structural system, respectively. $\ddot{\boldsymbol{X}}(\boldsymbol{\Theta}, t)$, $\dot{\boldsymbol{X}}(\boldsymbol{\Theta}, t)$ and $\boldsymbol{X}(\boldsymbol{\Theta}, t)$ represent the $n \times 1$ acceleration, velocity and displacement vectors of the structural system, respectively. $\ddot{x}_g(\boldsymbol{\Theta},\ t)$ represents the non-stationary stochastic seismic earthquakes which are generated by the spectral representation approach. The randomness of the structural parameters and ground motions is embedded in the random vector, $\boldsymbol{\Theta}$, which includes N groups of independent random variables (e.g., material, load, phase angle).

The Eq. 5 is suitable for arbitrary structural systems, and the theory of probability preservation is satisfied during the analysis with the randomness depicted by $\boldsymbol{\Theta}$. More generally, the $\boldsymbol{X}(\boldsymbol{\Theta}, t)$ can be referred to any concerned physical response in the structural systems relying on the random vector $\boldsymbol{\Theta}$. Call for the generalized PDEM equation based on the principle of probability preservation (Eq. 6):

$$\frac{\partial p_{\boldsymbol{X\Theta}}(\boldsymbol{X},\ \boldsymbol{\Theta},\ t)}{\partial t} + \dot{\boldsymbol{X}}(\boldsymbol{\Theta}, t) \cdot \frac{\partial p_{\boldsymbol{X\Theta}}(\boldsymbol{X},\ \boldsymbol{\Theta},\ t)}{\partial \boldsymbol{X}} = 0 \tag{6}$$

in which t represents the generalized time that reflects the evolutional direction. Worth noticing is that with regard to the equivalent extreme-value event in PDEM, a virtual stochastic process is required to be constructed, and t can be the virtual time. Besides, the initial condition of the structural system can be obtained as (Eq. 7):

$$p_{\boldsymbol{X\Theta}}(\boldsymbol{X},\ \boldsymbol{\Theta},\ t)|_{t=t_0} = \delta(\boldsymbol{X} - \boldsymbol{X}_0)p_{\boldsymbol{\Theta}}(\boldsymbol{\Theta}) \tag{7}$$

in which $\delta(\cdot)$ represents the Dirac function. $\boldsymbol{X}_0$ represents the deterministic value of the concerned physical response at the initial t_0. Then the PDF of the concerned physical response along with the generalized time t can be written as (Eq. 8):

$$p_{\boldsymbol{X}}(\boldsymbol{X}, t) = \int_{\Omega_{\boldsymbol{\Theta}}} p_{\boldsymbol{X\Theta}}(\boldsymbol{X},\ \boldsymbol{\Theta},\ t) d\boldsymbol{\Theta} \tag{8}$$

The above-mentioned generalized PDEM equation can be solved by a numerical approach or analytical approach. Considering that the target variable $\boldsymbol{X}(\boldsymbol{\Theta}, t)$ is affected by complicated dynamic behaviors of the structural system, Eq. 6 is difficult to express in an explicit form. Thus, the numerical procedure is adopted consequently. During the analysis, the representing points are required to be determined first, and a generalized F-Discrepancy method proposed by Li and Chen is selected [35, 49]. Assuming that for each earthquake level IM_α, the number of stochastic variables is m, the number of representing points is n_{set} in the domain $\Omega_{\boldsymbol{\theta}}$, then the point sets can be expressed as $\boldsymbol{\theta}_i = \{\boldsymbol{\theta}_{1,i}, \boldsymbol{\theta}_{2,i}, ..., \boldsymbol{\theta}_{m,i}\},\ i = 1, 2, ..., n_{set}$. The concerned physical variable in the structural system (e.g., CPI in this paper) is re-written as $CPI(\boldsymbol{\theta}, t)$, and the corresponding assigned probability for each probability space is denoted as P_i. For each point set $\boldsymbol{\theta}_i$, the deterministic dynamic and static analyses are performed to get the derivative of the concerned physical variable, i.e., $C\dot{P}I(\boldsymbol{\theta}_i, t)$, and the value is brought into Eq. 6 to realize the discretized form of the generalized PDEM equation, say (Eq. 9):

$$\frac{\partial p_{CPI,\boldsymbol{\theta}_i}(CPI,\ \boldsymbol{\theta}_i,\ t)}{\partial t} + C\dot{P}I(\boldsymbol{\theta}_i, t) \cdot \frac{\partial p_{CPI,\boldsymbol{\theta}_i}(CPI,\ \boldsymbol{\theta}_i,\ t)}{\partial CPI} = 0 \tag{9}$$

The numerical solution of Eq. 9 can be then realized via difference method [e.g., Lax-Wendroff (L-W) form or total variation (TV) form [50]] to acquire the $p_{CPI,\boldsymbol{\theta}_i}(CPI,\ \boldsymbol{\theta}_i,\ t)$. The numerical integration is conducted afterwards to get the PDF of the target variable of the structural system as follows (Eq. 10):

$$p_{CPI}(CPI, t) = \sum_{i=1}^{n_{set}} p_{CPI,\boldsymbol{\theta}_i}(CPI,\ \boldsymbol{\theta}_i,\ t) \tag{10}$$

In this stochastic analysis, an equivalent extreme-value event in PDEM is constructed and t is the virtual time without physical meaning. The results in Eq. 10 is then substituted into Eq. 4 for each earthquake level IM_α to acquire the PDEM-based probabilistic fragility relationship.

It is noteworthy that the above-mentioned analysis is set for the earthquake level $IM_\alpha, \alpha = 1, 2, ..., Tar$, and Tar represents the total number of earthquake levels in the analysis. The number of the representing points n_{set} is also for the earthquake level IM_α, followed with the number of generated non-stationary stochastic earthquake of n_{set} at this intensity. Thus, the information of the non-stationary stochastic earthquake [e.g., peak ground acceleration (PGA)] can also be the treated as the concerned physical variable and meets the principle of probability preservation, say, $PGA_\alpha = \{PGA_{1,\alpha}, PGA_{2,\alpha}, ..., PGA_{n_{set},\alpha}\}$, $\alpha = 1, 2, ..., Tar$. Thus, the PGA_α can also be brought into Eq. 6 to realize the discretized form of the generalized PDEM equation, as presented in Eq. 11 and 12.

$$\frac{\partial p_{PGA_\alpha,\boldsymbol{\theta}_i}(PGA_\alpha,\ \boldsymbol{\theta}_i,\ t)}{\partial t} + P\dot{G}A_\alpha(\boldsymbol{\theta}_i, t) \cdot \frac{\partial p_{PGA_\alpha,\boldsymbol{\theta}_i}(PGA_\alpha,\ \boldsymbol{\theta}_i,\ t)}{\partial PGA_\alpha} = 0 \tag{11}$$

$$p_{PGA_\alpha}(PGA_\alpha, t) = \sum_{i=1}^{n_{set}} p_{PGA_\alpha,\boldsymbol{\theta}_i}(PGA_\alpha,\ \boldsymbol{\theta}_i,\ t) \tag{12}$$

Herein the equivalent extreme-value event in PDEM is also constructed to acquire the PDEM-based probabilistic hazard relationship. With this step, the representative hazard value for the earthquake level IM_α with different exceeding probability is obtained, which responds to the corresponding fragility (via CPI) as presented in Eq. 9 and 10. Because the calculated probabilistic hazard results and probabilistic fragility results are derived from same probability space, a consistent 3-dimensional PDEM-based probabilistic hazard-fragility curves can be established. Compared with the traditional 2-dimensional fragility curves, the consistent 3-dimensional hazard-fragility curves increase a new axis as the exceeding probability of hazard intensity, and directly combines the hazard level to the fragility results through the same ground motions. The PDEM avoids the pre-defined distribution types and is more accurate than the lognormal assumption. The non-stationary stochastic ground motion avoids the wave selection process and reflects more reality than natural ground motions. The PDEM and non-stationary stochastic ground motions are the core links in the analysis to realize the consistency. The principles of the non-stationary stochastic ground motions are introduced in the following subsection. Fig. 1 shows the distinct flowchart of the proposed consistent seismic hazard and fragility analysis via PDEM, and Fig. 2 shows the detailed schematic steps in the analysis.

3. Modeling of non-stationary ground motions

In this paper, the non-stationary stochastic acceleration time series are obtained through the spectral representation of random functions as well as the stochastic process theory [51, 52]. In comparison with the natural ground motions and the stationary ground motions, the non-stationary stochastic ground motions contain more adjustable factors such as soil damping and angular frequency, and regard the spectral density as a time-changing element, thus a more accurate earthquake input process can be realized with combined intensity and frequency uncertainty [53, 54]. In addition, a modication procedure is adopted to adjust the spectral representation function, thus the mean acceleration spectra of individual earthquake samples and the target spectra can match ideally with less discreteness. The relevant generating equations are shown as follows.

The core part in the spectral representation approach to generate non-stationary stochastic earthquakes is the evolutionary power spectral density (EPSD). In this paper, the Clough-Penzien bilateral EPSD function $[S_{\ddot{X}_g}(t, \omega)]$ which contains the intensity non-stationarity and frequency non-stationarity is adopted, as presented in Eq. 13 [55, 56]:

$$S_{\ddot{X}_g}(t, \omega) = A^2(t) \cdot \frac{\omega_g^4(t) + 4\xi_g^2(t)\omega_g^2(t)\omega^2}{\left[\omega^2 - \omega_g^2(t)\right]^2 + 4\xi_g^2(t)\omega_g^2(t)\omega^2} \cdot \frac{\omega^4}{\left[\omega^2 - \omega_f^2(t)\right]^2 + 4\xi_f^2(t)\omega_f^2(t)\omega^2} \cdot S_0(t) \tag{13}$$

where $\omega_g(t)$, $\xi_g(t)$, $\omega_f(t)$ and $\xi_f(t)$ represent the site non-stationarity of EPSD with time-varying characteristics of earthquake frequency, as presented in Eq. 14 and Eq. 15:

$$\omega_g(t) = \omega_0 - a\frac{t}{T}, \quad \xi_g(t) = \xi_0 + b\frac{t}{T} \tag{14}$$

$$\omega_f(t) = 0.1\omega_g(t), \quad \xi_f(t) = \xi_g(t) \tag{15}$$

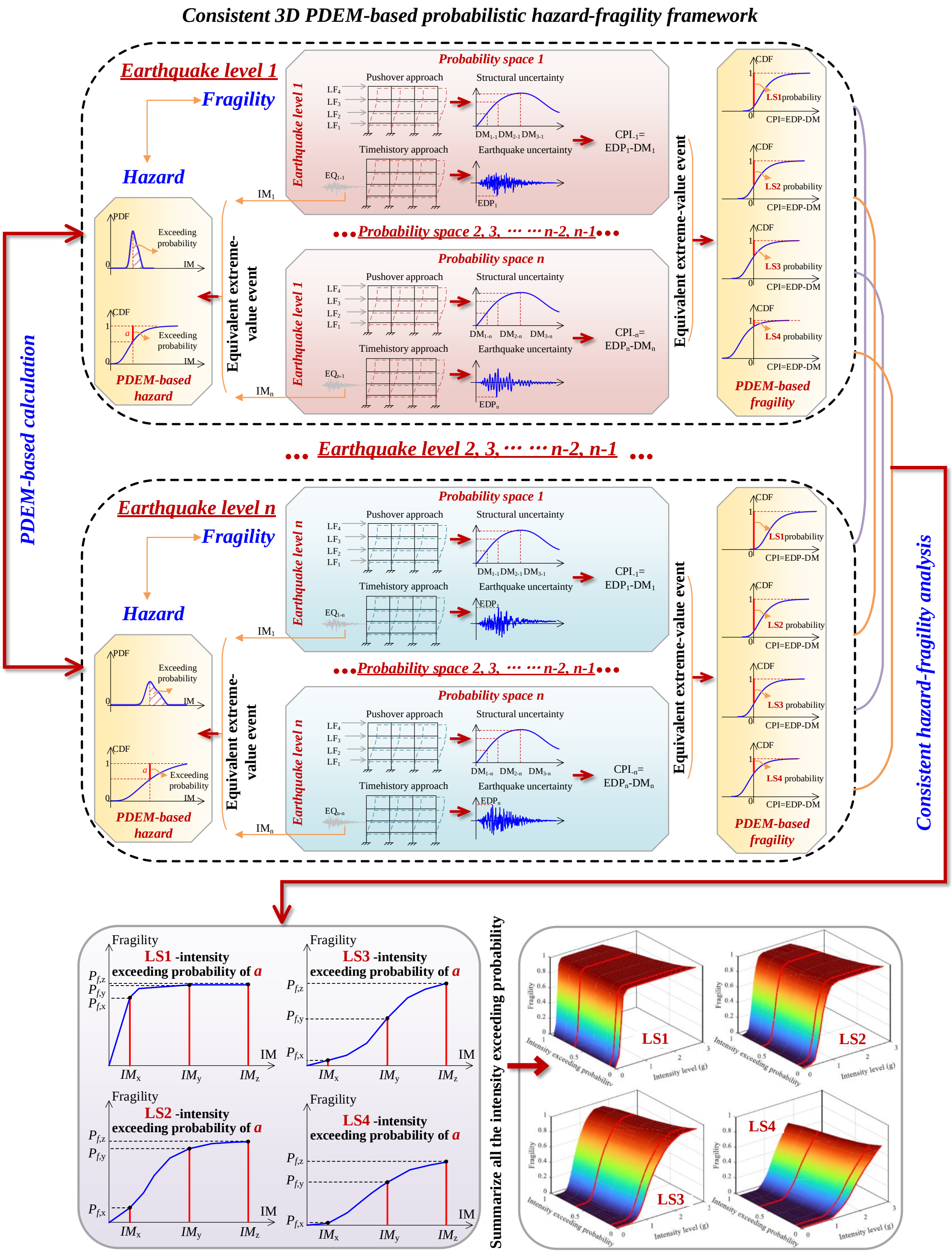

Figure 2: The detailed schematic steps of the consistent seismic hazard and fragility analysis via PDEM

where ω_0 and ξ_0 reflect the information of primary site angular frequency and soil damping ratio, respectively. T denotes the duration time of the non-stationary stochastic earthquakes. a denotes the field classification parameter, while b denotes the seismic group parameter.

In addition, the $A(t)$ and $S_0(t)$ in Eq. 13 denote the intensity adjusting parameter and spectral intensity parameter, respectively. According to Ou and Wang [57], a unimodal envelope expression is adopted herein, as expressed in Eq. 16 and Eq. 17.

$$A(t) = \left[\frac{t}{c} \cdot exp(1 - \frac{t}{c}) \right]^d \tag{16}$$

$$S_0(t) = \frac{\bar{a}^2_{\max}}{\gamma^2 \pi \omega_g(t) \cdot \left[2\xi_g(t) + 1/(2\xi_g(t)) \right]} \tag{17}$$

where c denotes the peak ground acceleration arrival point, and d denotes the shape controlling indicator of the intensity adjusting function $[A(t)]$. γ denotes the equivalent maximum parameter of peak ground acceleration, and $\bar{a}_{\max}$ reflects the average value of peak ground acceleration. Under different design group and site classification, the values of the above parameters will vary, and the summarization of the relevant recommendation values can be available from Liu et al [58].

With the expression of Clough-Penzien bilateral EPSD function in Eq. 13, the zero-mean non-stationary stochastic acceleration time series can be formed, as expressed in Eq. 18 [59, 60]:

$$\ddot{X}_g(t) = \sum_{k=1}^{N} \sqrt{2S_{\ddot{X}_g}(t, k\Delta\omega) \cdot \Delta\omega} \cdot \left[\cos(k\Delta\omega t) X_k + \sin(k\Delta\omega t) Y_k \right] \tag{18}$$

where $\Delta\omega$ denotes the interval frequency that is determined by the truncated frequency and items (N). In Eq. 18, the total number of random variables is $2N$ (i.e., $\{X_1, Y_1\} \ldots \{X_N, Y_N\}$), and $\{X_k, Y_k\}$ $(k = 1, 2, ..., N)$ denote the standard orthogonal stochastic variables. To reduce the random variables in the earthquake generation process and to improve the calculation efficiency, a deterministic mapping procedure of two standard orthogonal stochastic variables $\{\bar{X}_n, \bar{Y}_n\}$ $(n = 1, 2, ..., N)$ is introduced to rearrange the values of $\{X_k, Y_k\}$. Worth mentioning is that if this process is ignored, the non-stationary stochastic earthquakes will show unreasonable bumps. $\{\bar{X}_n, \bar{Y}_n\}$ can be composed with multiple forms, and in this paper, the non-Gaussian orthogonal expression with two independent stochastic variables (i.e., Θ_1 and Θ_2) are adopted as shown in Eq. 19, thus the number of random variables is reduced from $2N$ to 2 [61, 62]. The values of fundamental variables Θ_1 and Θ_2 vary from 0 to 2π under the assumption of uniform distributions.

$$\bar{X}_n = sin(n\Theta_1) + cos(n\Theta_1), \; \bar{Y}_n = sin(n\Theta_2) + cos(n\Theta_2) \tag{19}$$

Moreover, to enhance the fit-extent between the mean acceleration spectra of individual earthquake samples and the target spectra, a modication procedure to the spectral density function is added in light of an iterative solution, as illustrated in Eq. 20:

$$S_{\ddot{X}_g}(t,\omega)|_{i+1} = \begin{cases} S_{\ddot{X}_g}(t,\omega), & 0 < \omega \le \omega_c \\ S_{\ddot{X}_g}(t,\omega)|_i \cdot \frac{AS^T(\omega,\xi)^2}{AS^M(\omega,\xi)^2|_i}, & \omega > \omega_c \end{cases} \tag{20}$$

where $S_{\ddot{X}_g}(t,\omega)|_{i+1}$ and $S_{\ddot{X}_g}(t,\omega)|_i$ denote the $(i+1)$th and ith iterative expression of spectral density functions, respectively. ω_c represents the limited frequency, and the exceeding sections (i.e., $\omega > \omega_c$) of the non-stationary stochastic earthquakes are required for adjustment. $AS^T(\omega, \xi)$ indicates the target acceleration spectrum, while $AS^M(\omega, \xi)|_i$ indicates the mean acceleration spectrum of generated stochastic motions after ith-iteration. ξ represents the damping ratio and the commonly-used recommendation is 0.05 for buildings. $\omega = 2\pi/T_s$, and T_s represents the fundamental structural period.

In this paper, 200 non-stationary stochastic ground motions are generated, and the phase angles (i.e., Θ_1 and Θ_2) of each ground motion are sampled according to the generalized F-Discrepancy method in PDEM. The fundamental earthquake level is set as 0.1 g, the soil type classification is type-C and the structural importance class is type-II according to the ASCE/SEI 7-10 [63], thus the corresponding values of stochastic parameter can be given (i.e., ω_0 is 13.5 s^{-1}, ξ_0 is 0.65, γ is 2.6, T is 25 s, a is 5 s^{-1}, b is 0.2, c is 6 s, and d is 2). The interval frequency $\Delta\omega$ is chosen as 0.15 rad/s, the truncated item N is determined as 1000, and the limited frequency ω_c is adopted as 1.57 $rad \cdot s^{-1}$. Fig. 3(a) displays the samples of non-stationary stochastic ground motions, and Fig. 3(b) compares the mean and target acceleration response spectra after modification. Fig. 3(c) and 3(d) show the mean values and standard deviations of non-stationary stochastic ground motions, respectively.

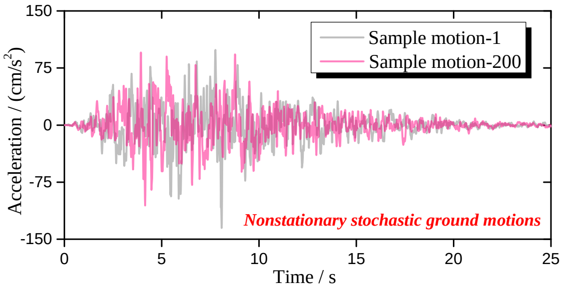

(a) Samples of non-stationary stochastic ground motion

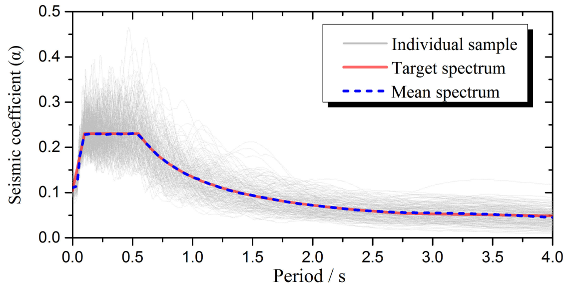

(b) Comparison between mean and target acceleration response spectra

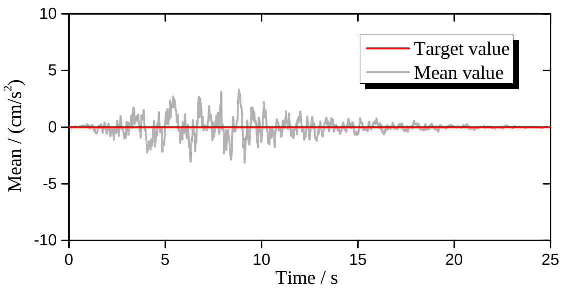

(c) Mean values of non-stationary stochastic ground motion

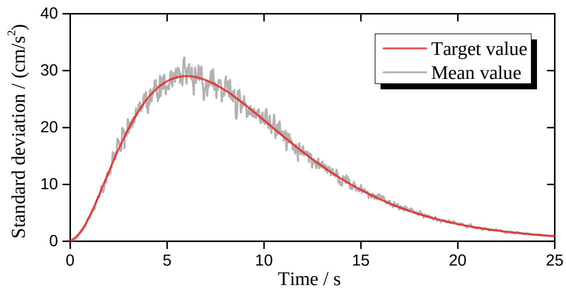

(d) Standard deviations of non-stationary stochastic ground motion

Figure 3: Non-stationary stochastic ground motions

4. Modeling of structures and associated uncertainties

To evaluate the damage states and conduct the performance calculations of reinforced concrete structures through non-stationary stochastic ground motions, a fiber-based numerical model using OpenSees software is established in this paper [64, 65]. The fiber-based numerical model is regarded to be computationally efficient and analytically accurate, and is widely accepted in the earthquake community for decades. In comparison with the macro model based on the solid elements, the fiber-based model reduces the time cost and meanwhile maintains the structural features, thus is especially significant for seismic fragility evaluation. Fig. 4 displays the typical modelling strategy of reinforced concrete frames (RCFs).

To characterize the nonlinear behaviors of beam and column components, the force-based fiber elements with distributed plasticity are adopted (i.e., nonlinearBeamColumn element in OpenSees), which is integrated through flexibility theory and distributes the element force along the length direction [66, 67]. Compared with the displacement-based fiber elements, the force-based fiber elements are more stable with the guaranteed equilibrium constraint, thus can be rather effective under intense nonlinearity and can reflect the structural property with fewer element number. The fiber cross-sectional models are assigned to the force-based elements, which divide the sections as steel and concrete fibers, respectively. The Steel02 constitutive material in OpenSees is defined for steel fibers, and the Concrete02 constitutive material in OpenSees is defined for Concrete fibers. As for the hoop effects of stirrups, a confined concrete model is considered for the core zones within stirrups [68]. An amplification factor (k) is introduced to increase the stress-strain relationship at these zones, as shown in Eq. 21. Besides, the ultimate strain of concrete will obviously affect the convergence performance and capacity variations of the structural system. Scott et al. [69] conservatively recommended the ultimate concrete strain in compression when the stirrups in core zones begin to break, and the equation is used as Eq. 21 for calculation, in which ρ_s and ε_{max} denote the volume stirrup ratio and the ultimate strain of confined concrete in compression, respectively. f_{yh} and $f_c^{'}$ denote the stirrup yielding strength and the cylinder compressive strength of concrete, respectively. As for the unconfined concrete, the corresponding ultimate compressive strain is adopted as 0.004.

$$k = 1 + \frac{\rho_s f_{yh}}{f_c^{'}}, \quad \varepsilon_{max} = 0.004 + 0.9\rho_s \cdot \frac{f_{yh}}{300} \tag{21}$$

To characterize the shear and bond-slip properties of beam-column joints, the Joint2D element in OpenSees is adopted herein to simulate the connections. The Joint2D element contains one central spring and four side springs, and can be regarded as a parallelogram shear board. The central spring controls the shear performance in the core zones, while the side springs control the bond-slip behaviors in the interface [70]. The pinching4 material in OpenSees is allocated to the central spring to reflect the core moment-rotation, and the hysteretic material in OpenSees is allocated to the side spring to reflect the interface moment-rotation. To be specific, the pinching4 material defines four points in each loading direction and incorporates the parameters to reflect stiffness degeneration as well as strength pinching. The corresponding point values can be determined through modified compression field theory [71]. The hysteretic material defines three points in each loading direction, accompanied with damage due to ductility and energy, and the corresponding point values can be determined through the unit-length fiber section analysis, in which the stress-strain model of Steel02 is substituted by stress-slip model (e.g., Bond_SP01 model in OpenSees) to discuss the bond-slip functions [72]. The stress-slip model can refer to Eq. 22, in which S_y and S_u represent the yielding slip and ultimate slip, respectively. β represents the local bond-slip parameter and is commonly recommended as 0.4. Compared with the rigid connections of beam and column elements at joints, which commonly overestimate the structural behaviors, the Joint2D element reflects more details and includes higher authenticity in the dynamic analysis. In addition, the EqualDOF constraint in OpenSees is used at the two outer Joint2D elements of each storey, for the purpose of binding the horizontal displacements under the rigid-storey assumption. The Joint2D element is the critical point in the simulation of RCFs, and the validation with experimental data [73] is given in the Fig. 4, which indicates an ideal fitting accuracy.

$$S_y = 2.54 \cdot \left[\frac{d}{8437} \cdot \frac{f_y}{\sqrt{f_c'}} \cdot (2\beta + 1) \right]^{1/\beta} + 0.34, \quad S_u = 35 \cdot S_y \tag{22}$$

As for the associated uncertainties in the modelling, two types of uncertainties are considered, which are the earthquake-related uncertainty and structural-related uncertainty. As mentioned before, the non-stationary stochastic earthquake model based on the spectral representation is adopted in this paper, and the ground motions are controlled by the phase angles (i.e., Θ_1 and Θ_2), thus the phase angles constitute the earthquake-related uncertainty. As for the structural-related uncertainty, three subtypes are considered (i.e, materials, dimensions, and loads). The material uncertainty includes the yielding strength, compressive strain, hardening ratio and so on. The dimension uncertainty includes the rebar diameter, storey height, sectional size, and so on. The load uncertainty includes the consistent live load, temporary live load, gravity load, and so on. After determining the uncertainty variables and distributions, the generalized F-Discrepancy method in PDEM is used to generate the samples, and the corresponding structural analysis with the numerical model as mentioned above is conducted. The detailed implementation of the proposed method will be introduced in the following parts.

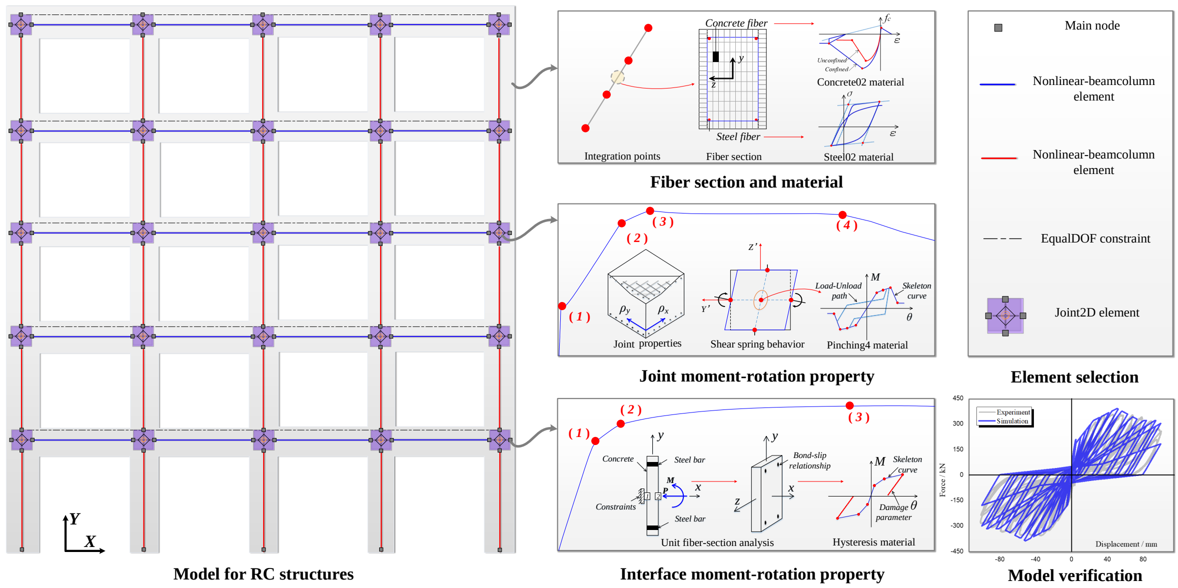

Figure 4: Modeling of structures and strategy of details

5. Implementation of the proposed method: Application into RCF

5.1. Design information and uncertainty

To implement the consistent seismic hazard and fragility analysis via PDEM, an application into RCF is conducted correspondingly. The prototype is designed through the code for concrete structures in China [74], which is a 3-span-6-storey RCF located in the site with fortification level of seven degree. The corresponding fortification PGA is 0.1 g, which means the exceeding probability of 10 % during 50 years. The span length is 6300 mm, and the storey heights for the first and other storeys are 4200 mm and 3500 mm, respectively. The soil type classification is type-C, and the structural importance class is type-II according to the ASCE/SEI 7-10 [63]. The design sectional sizes of beams and columns are 350 $\times$ 550 mm and 650 $\times$ 650 mm, respectively. For the storey 1 to 3, the rebar diameters are designed as 25 mm at both sectional sides for columns, and designed as 20 mm at both sectional sides for beams. For the storey 4 to 6, the rebar diameters are designed as 20 mm at both sectional sides for columns, and designed as 18 mm at both sectional sides for beams. The concrete is type-C30, with the design compressive strength of 14.3 MPa, and the reinforcing steel is type-HRB335, with the design yielding strength of 300 MPa. As for the constructional steel and stirrup, the adopted type is HPB300 with the design yielding strength of 270 MPa. The detailed design information and constructional dimensions are presented in Fig. 5.

The numerical model of the prototype 3-span-6-storey RCF is established by the approach in Section 4. Lumped mass is considered at joints and the damping ratio is delimited as 5 %. The fundamental period with the designed information is 0.956 s. With regard to the earthquake-related and structural-related uncertainties, totally 26 random variables are selected and the distribution parameters are listed in Tab. 1. For the initial earthquake level, 200 sample sets (i.e., earthquake and structure pairs) with different assigned probability are generated for numerical simulation. Then the deterministic static pushover analysis is performed to capture the limit states (i.e., capacity) in each probability space, and the deterministic dynamic time-history analysis is performed to capture the structural responses (i.e., demand) in each probability space. Both the capacity and demand are reflected by the maximum interstorey drift ratio (MIDR), which is a commonly used index for RCF assessment. As for the capacity, four performance levels are defined, i.e., slight, moderate, extensive, and collapse. The slight state corresponds to the MIDR of first steel yield, the moderate state corresponds to the MIDR via equivalent energy principle, the extensive state corresponds to the MIDR of the peak capacity, and the collapse state corresponds to the MIDR of the 85 % of peak capacity. The detailed definition methods are not elaborated herein and can be accessible from Cao et al [75, 76]. After that the CPI as mentioned in Section 2 is calculated and summarized for subsequent analysis via PDEM. In addition, the PGA and $S_a(T_1)$ of the 200 non-stationary stochastic earthquakes for this earthquake level are also obtained correspondingly. The earthquake level continues to increase until the target level and the above steps are repeated for each earthquake level.

A noteworthy point herein is that in this paper, the global capacities of the overall structures are adopted (i.e., via the damage measure of MIDR). The global capacities contain certain advantages such as rapid assessment of structural performance after hazards or efficient evaluation of damage levels for decision making, as recommended in Hazus [77]. At this stage, a series of approaches of employing local member / section / joint capacity checks have been proposed by researchers. These local-capacity based approaches are commonly more accurate and authentic. For instance, according to the FEMA P-58 procedure [78], the structural losses and risks are calculated via the accumulation of component-induced probabilistic behaviors. Villaverde [79] gave the state-of-the-art review of the seismic collapsing capacities for structural buildings, in which the balance and significance between the local and global capacities were detailedly analyzed and systematically summarized. Kazantzi et al. [80] performed the seismic evaluation of a moment resisting frame under the combined strength-ductility uncertainties, and the local failure indexes as well as the local demand-capacity correlations were both considered. The research found that the local damage estimations affected the overall structural responses to some degree. Freddi et al. [81] adopted the local indexes to give a more thorough and realistic characterization of failure patterns of low ductility frames without seismic reinforcements. The corresponding probabilistic seismic demand models were established, and during the process the distribution types as well as the regression models were well investigated. In this paper, the authors just hope to adopt the global capacities as an example to present the strategy of how to establish the 3D consistent non-parametric seismic hazard-fragility framework via PDEM, as well as to analyze the corresponding influence under the combined capacity-demand uncertainties via PDEM. In the further in-depth research, the extensions to the local member / section / joint capacities via PDEM can be straightforward for a better application and clearer interpretation.

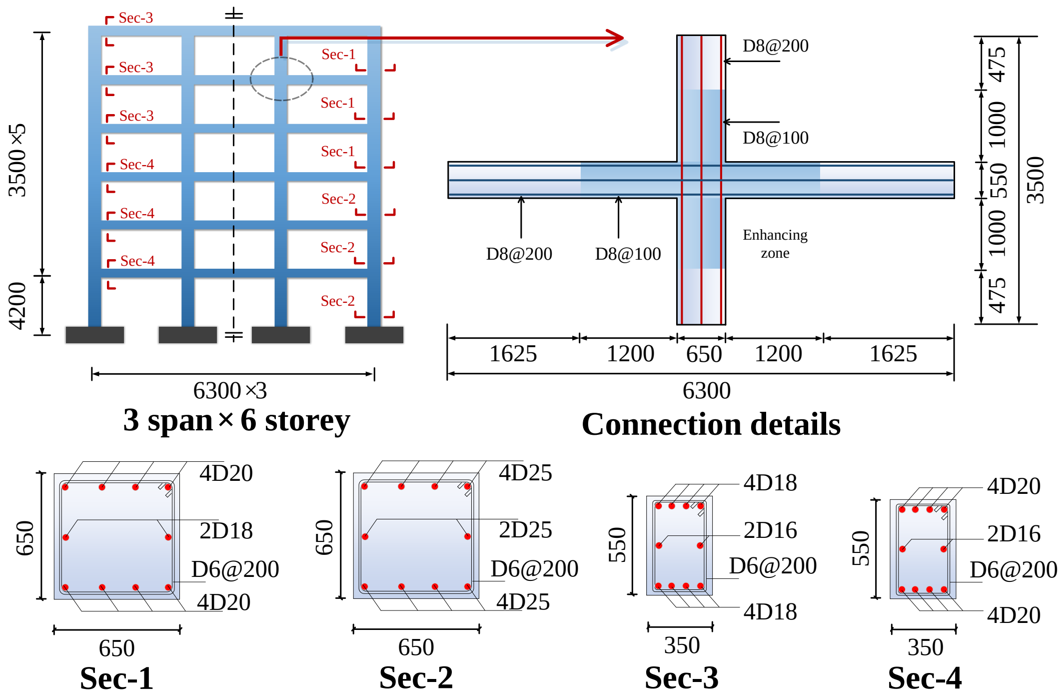

Figure 5: The detailed design information and constructional dimensions in application

Table 1: The random variables and distribution parameters

Random variables	***Symbol***	***Distribution***	***Mean***	***COV***	***Source***
Stochastic motion parameter	$\Theta 1$	Uniform	3.142 (1)	0.577	[82]
Stochastic motion parameter	$\Theta 2$	Uniform	3.142 (1)	0.577	[82]
Concrete bulk density	γ	Normal	26.5 (kN/m^3)	0.0698	[75]
Storey consistent live load	L_{c1}	Gumbel	0.386 (kN/m^2)	0.464	[83]
Storey temporary live load	L_{t1}	Gumbel	0.356 (kN/m^2)	0.683	[83]
Roof consistent live load	L_{c2}	Gumbel	0.504 (kN/m^2)	0.321	[83]
Roof temporary live load	L_{t2}	Gumbel	0.468 (kN/m^2)	0.538	[83]
Beam span	sb	Normal	6300 (mm)	0.003	[84]
First storey height	hf	Normal	4200 (mm)	0.003	[84]
Standard storey height	ha	Normal	3500 (mm)	0.003	[84]
Column height	hc	Normal	650 (mm)	0.01	[84]
Beam height	hb	Normal	550 (mm)	0.01	[84]
Beam width	wb	Normal	350 (mm)	0.01	[84]
Slab height	hs	Normal	120 (mm)	0.01	[42]
Core concrete compressive strength	$f_{cp,core}$	Lognormal	33.6 (MPa)	0.21	[42]
Core concrete peak strain	$\varepsilon_{cp,core}$	Lognormal	0.0022 (1)	0.17	[42]
Core concrete ultimate strain	$\varepsilon_{cu,core}$	Lognormal	0.0113 (1)	0.52	[42]
Cover concrete compressive strength	$f_{cp,cover}$	Lognormal	26.1 (MPa)	0.14	[42]
Cover concrete ultimate strain	$\varepsilon_{cu,cover}$	Lognormal	0.004 (1)	0.2	[42]
Rebar diameter in columns	$d25$	Normal	25 (mm)	0.04	[84]
Rebar diameter in beams	$d20$	Normal	20 (mm)	0.04	[84]
Rebar diameter in beams	$d18$	Normal	18 (mm)	0.04	[84]
Rebar yielding strength	f_y	Lognormal	378 (MPa)	0.074	[85]
Rebar elastic modulus	E	Lognormal	201000 (MPa)	0.033	[85]
Rebar hardening ratio	b	Lognormal	0.02 (1)	0.2	[85]
Damping ratio	ς	Normal	0.05 (1)	0.1	[42]

5.2. Virtual stochastic process of PDEM

During the equivalent extreme-value event in PDEM, a virtual stochastic process is commonly required to be constructed for the extreme-value analysis. As mentioned in the Eq. 6, the parameter t represents the generalized time that reflects the evolutional direction. In the virtual stochastic process of PDEM, t is commonly regarded as the virtual time varying from 0 to 1. As for different stochastic conditions in consideration, the actual time to achieve the extreme-value is not the same (e.g., the earthquake time to reach MIDR in this example), so we assume that all the extreme-values of different stochastic conditions appear at the virtual time 1 under the virtual stochastic process of PDEM (and time 0 is the initial state). During the virtual stochastic process of PDEM, the PDF or CDF of extreme-value is the primary focus, and the corresponding time-history development is not the main point. More details related to the virtual stochastic process of PDEM can be found in Li et al. [86] and Chen et al. [87].

Fig. 6 and Fig. 8 present the PDF, CDF and hazard curves of PGA for different earthquake levels via PDEM, and Fig. 7 and Fig. 9 present the PDF, CDF and hazard curves of $S_a(T_1)$ for different earthquake levels via PDEM. During the analysis, the virtual stochastic process is well established. To be specific, Fig. 6(a) to 6(f) present the CDF and exceeding probability of PGA for intensity of 0.1 g, 0.2 g, 0.3 g, 0.5 g, 1.0 g, and 2.0 g, respectively, and Fig. 7(a) to 7(f) present the CDF and exceeding probability of $S_a(T_1)$ for these intensities. The black dotted line indicates the CDF value while the red lines indicate the exceeding probability of intensity [PGA or $S_a(T_1)$]. Totally three levels of exceeding probability of PGA or $S_a(T_1)$ for each intensity are marked (i.e., 63.2 %, 10 % and 2 %), which corresponds to the frequent earthquake level, fortification earthquake level, and rare earthquake level, respectively. For instance, for the intensity of 1.0 g, the PGA of frequent earthquake level is given as 1.0134 g, the PGA of fortification earthquake level is given as 1.3007 g, and the PGA of rare earthquake level is given as 1.4039 g. For the intensity of 1.0 g, the $S_a(T_1)$ of frequent earthquake level is given as 0.8504 g, the $S_a(T_1)$ of fortification earthquake level is given as 1.3693 g, and the $S_a(T_1)$ of rare earthquake level is given as 1.6542 g. Through this way, the representative PGA or $S_a(T_1)$ for each earthquake level is assigned with the probabilistic meaning and can be connected to the subsequent fragility analysis to constitute the consistent hazard-fragility curves. Fig. 8(a) and 9(a) present the PDF of PGA or $S_a(T_1)$ for each earthquake level, and it can be observed that the PDF tendency becomes flattened from intensity of 0.1 g to 2.0 g. Although the shape of the PDF via PDEM is similar to the lognormal assumptions in the smaller intensity, the tendency shows difference with the intensity increasing (e.g., non-smooth curve), which can also be found in Ning [29]. Fig. 8(b) and 9(b) present the hazard curves of PGA or $S_a(T_1)$ for each earthquake level. From these two subfigures, it can be observed that the curves move towards right with the intensity increasing, and the representative values for different earthquake levels with the various probabilistic meaning can be acquired, in order to combine with the later fragility evaluation. A noteworthy point is that the hazard curve herein is reflected as the exceeding probability of PGA or $S_a(T_1)$ for each earthquake level according to the PDEM theory, and it differs from the mean annual rate or annualized probability of exceeding a given level of the intensity measure in expression.

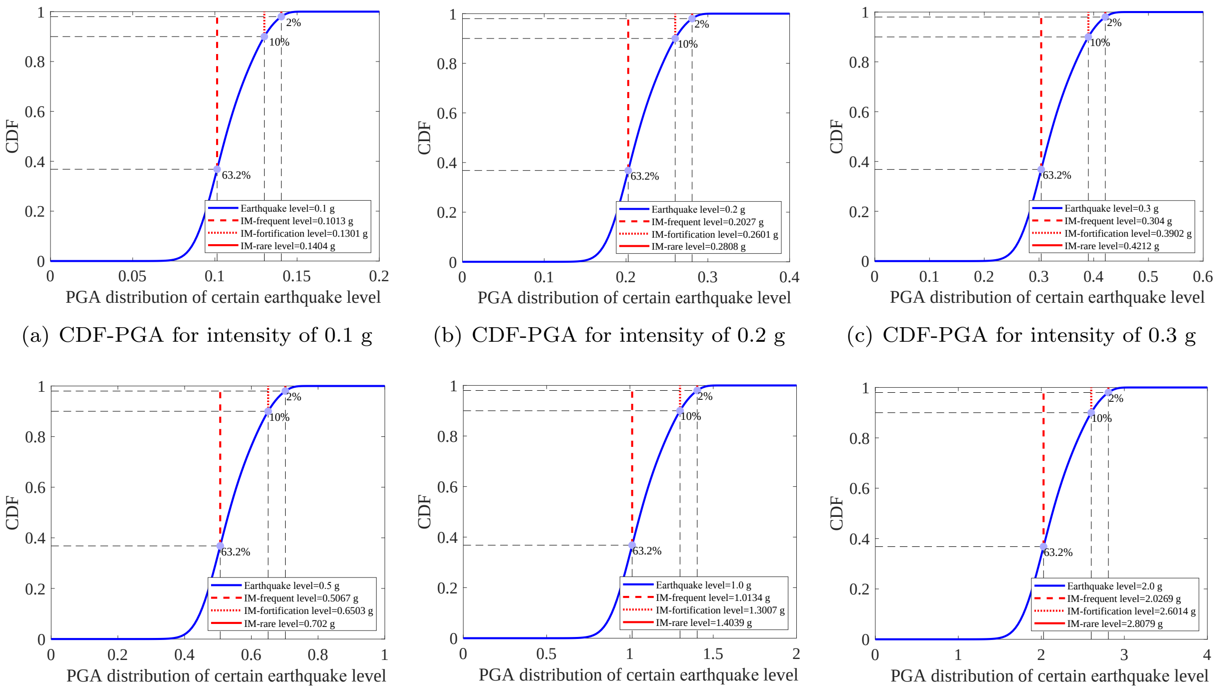

(a) CDF-PGA for intensity of 0.1 g (b) CDF-PGA for intensity of 0.2 g (c) CDF-PGA for intensity of 0.3 g

(d) CDF-PGA for intensity of 0.5 g (e) CDF-PGA for intensity of 1.0 g (f) CDF-PGA for intensity of 2.0 g

Figure 6: The CDF of PGA for different earthquake levels via PDEM

Fig. 10 presents the CDF of CPI (i.e., demand of MIDR minus capacity of MIDR) and fragility for different limit states and earthquake levels via PDEM, and the virtual stochastic process is established during the analysis. Fig. 10(a) to 10(d) present the results of slight state for intensity of 0.1 g, 0.5 g, 1.0 g and 2.0 g. Correspondingly, Fig. 10(e) to 10(h), Fig. 10(i) to 10(l), and Fig. 10(m) to 10(p) present the results of moderate state, extensive state, and collapse state for different intensities, respectively. The black dotted line indicates the CDF value of CPI while the red solid line indicates the fragility result at this level. According to Section 2, the values should correspond to the CPI=0. After connecting the fragility results (i.e., red lines) in Fig. 10 and linking to the PGA (in Fig. 6) or $S_a(T_1)$ (in Fig. 7) with the same exceeding probability, the fragility curves are generated, as displayed in Fig. 11. The subfigures 11(a), 11(c) and 11(e) indicate the fragility with different PGA exceeding probability of 63.2 %, 10 %, and 2 %, respectively, and the subfigures 11(b), 11(d) and 11(f) indicate the fragility with different $S_a(T_1)$ exceeding probability of 63.2 %, 10 %, and 2 %, respectively. The median values (with fragility of 50 %) are also marked in Fig. 11. Take the Fig. 11(a) and earthquake level of 1.0 g as an example, the corresponding fragility results of slight,

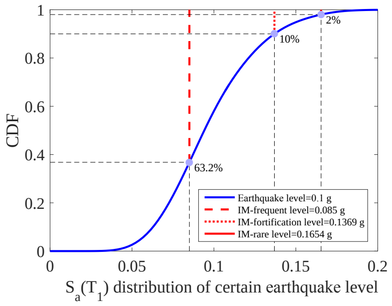

(a) CDF-$S_a(T_1)$ for intensity of 0.1 g

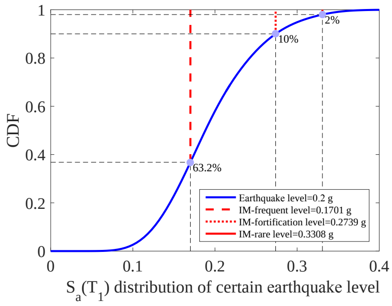

(b) CDF-$S_a(T_1)$ for intensity of 0.2 g

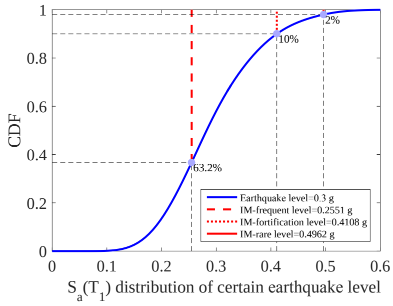

(c) CDF-$S_a(T_1)$ for intensity of 0.3 g

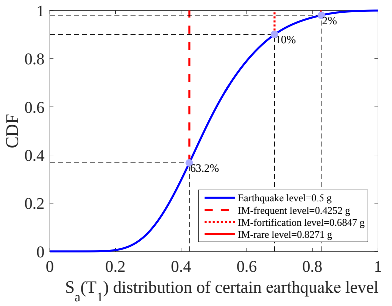

(d) CDF-$S_a(T_1)$ for intensity of 0.5 g

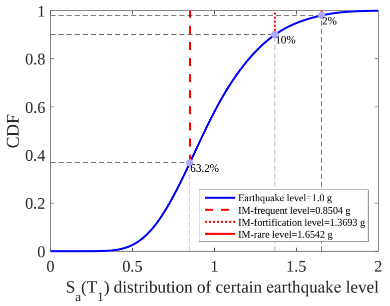

(e) CDF-$S_a(T_1)$ for intensity of 1.0 g

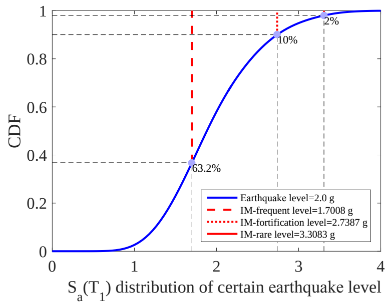

(f) CDF-$S_a(T_1)$ for intensity of 2.0 g

Figure 7: The CDF of $S_a(T_1)$ for different earthquake levels via PDEM

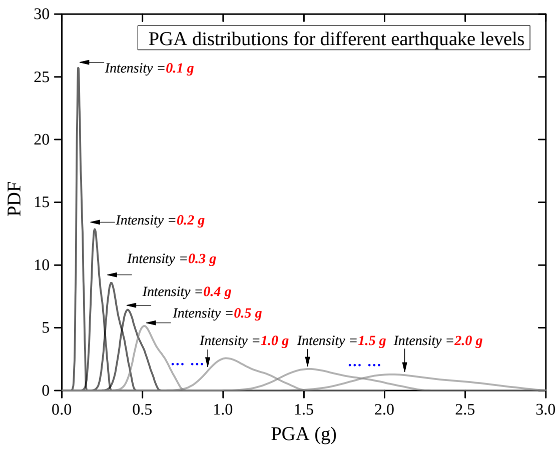

(a) PDF of PGA for each earthquake level

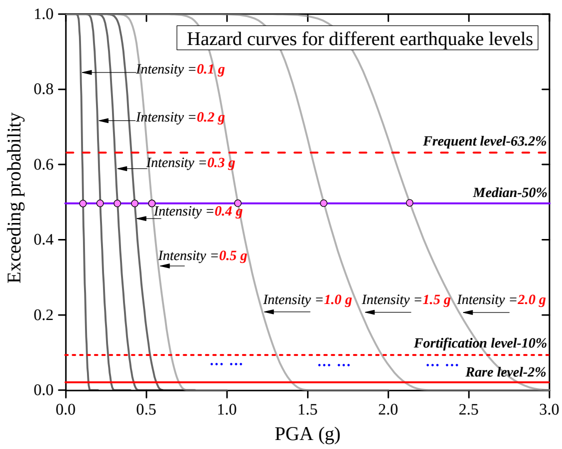

(b) Hazard curves of PGA for each earthquake level

Figure 8: The PDF and hazard curves of PGA for different earthquake levels via PDEM

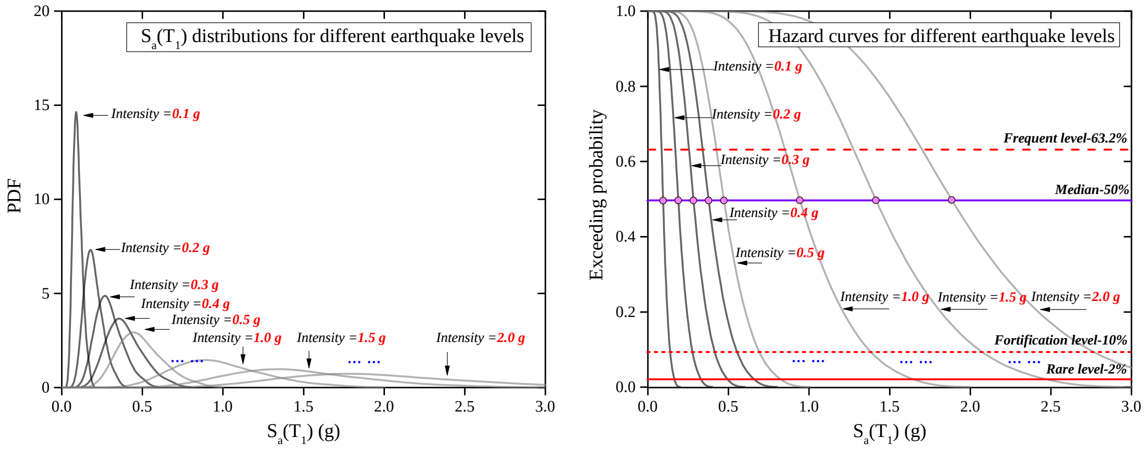

(a) PDF of $S_a(T_1)$ for each earthquake level

(b) Hazard curves of $S_a(T_1)$ for each earthquake level

Figure 9: The PDF and hazard curves of $S_a(T_1)$ for different earthquake levels via PDEM

moderate, extensive and collapse states can be obtained as 0.9951, 0.9944, 0.6414, and 0.0912 from Fig. 10(c), 10(g), 10(k) and 10(o), respectively. For the PGA exceeding probability of 63.2 % at this earthquake level (i.e., frequent earthquake level), the corresponding representative PGA is obtained as 1.0134 g, as displayed in Fig. 6(e), and for the $S_a(T_1)$ exceeding probability of 63.2 % at this earthquake level, the corresponding representative $S_a(T_1)$ is obtained as 0.8504 g, as displayed in Fig. 7(e). These data are also marked in Fig. 11 in gray lines and then the fragility points to curves are generated subsequently.

5.3. *Consistent 3D hazard-fragility curves*

In light of the PDEM-based consistent seismic hazard and fragility theories introduced in Section 2, Fig. 12 and 13 present the consistent 3D PDEM-based probabilistic hazard-fragility curves for different limit states, based on the PGA and $S_a(T_1)$, respectively. The red lines in each subfigure indicate the fragility curves with the PGA or $S_a(T_1)$ exceeding probability of 63.2 % (frequent level), 10 % (fortification level) and 2 % (rare level), as depicted in Fig. 11. The color bar reflects the fragility values from 0 to 1. Through the 3D consistent hazard-fragility curves, the exceeding probability for different limit states under different earthquake levels can be predicted, and the earthquake levels are assigned with different exceeding probability to build a connection with the hazard extent. With the introduction of the PDEM and non-stationary stochastic process into the PBEE, the 3D non-parametric hazard-fragility curve is realized, and the probabilistic relationship from hazard to fragility is consistent, directly meeting the conditional probability in the full-probability formula of the risk-based PBEE framework. Generally, this approach provides new ideas for the consistent risk-based assessment scheme in the PBEE, and provides references for the non-parametric probabilistic hazard analysis or fragility analysis in the future study.

Worth mentioning herein is that the implementation of the PDEM-based hazard or fragility approach relies on the representative points in probability space, and its superiority is that there is no need to pre-define the shape of the curve forms, and at the same time it has the ideal calculation results. To be specific, the PDEM-based approach avoids the lognormal distribution assumption of demand or capacity in the classic expression, while the lognormal distribution assumption may not be satisfied under highly nonlinear scenarios thus leading to inaccurate probabilistic curves in PBEE [88, 89]. However, as for the problems such as the efficiency to accuracy ratio or total calculation times, the PDEM-based approach may not be competitive. For example, when the classic lognormal-based approach is coupled with the cloud analysis, the calculation efficiency may be better than the PDEM-based approach. Some references can be available in Kennedy and Ravindra [90], Jalayer and Cornell [91], Lallemant et al. [92], Baker [93], and Bakalis and Vamvatsikos [94]. This aspect is not further discussed in this study, because this paper aims at providing

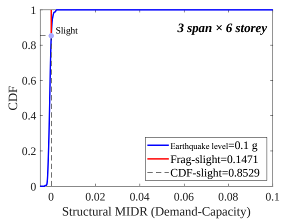

(a) Intensity of 0.1 g

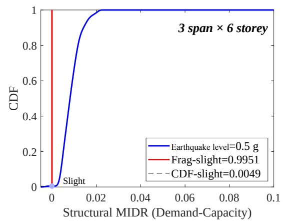

(b) Intensity of 0.5 g

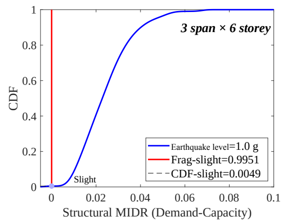

(c) Intensity of 1.0 g

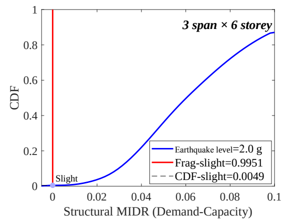

(d) Intensity of 2.0 g

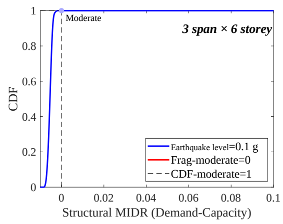

(e) Intensity of 0.1 g

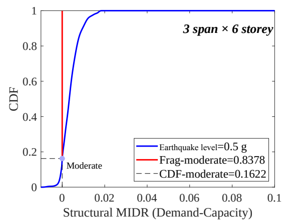

(f) Intensity of 0.5 g

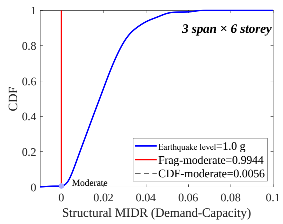

(g) Intensity of 1.0 g

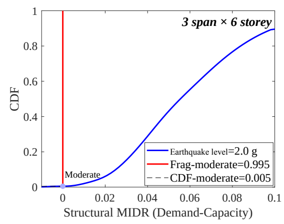

(h) Intensity of 2.0 g

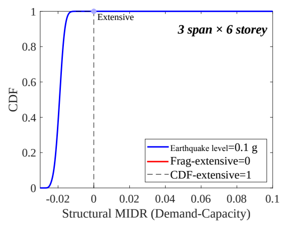

(i) Intensity of 0.1 g

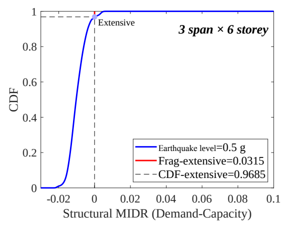

(j) Intensity of 0.5 g

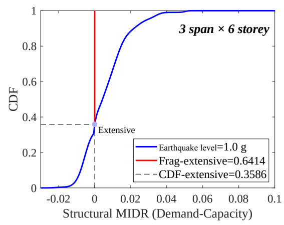

(k) Intensity of 1.0 g

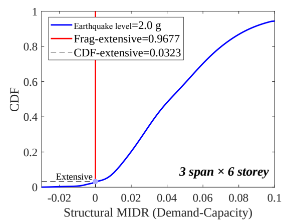

(l) Intensity of 2.0 g

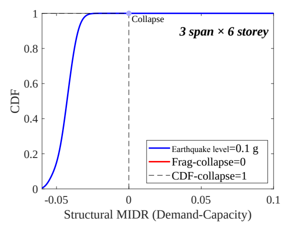

(m) Intensity of 0.1 g

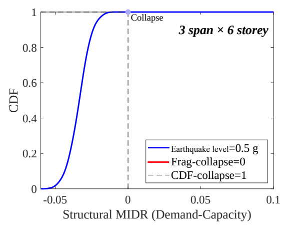

(n) Intensity of 0.5 g

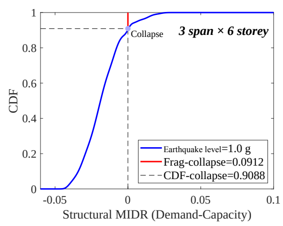

(o) Intensity of 1.0 g

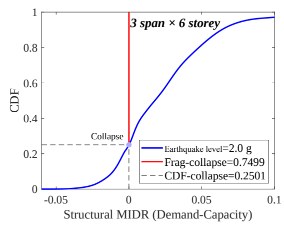

(p) Intensity of 2.0 g

Figure 10: The CDF of CPI and fragility for different limit states and earthquake levels via PDEM

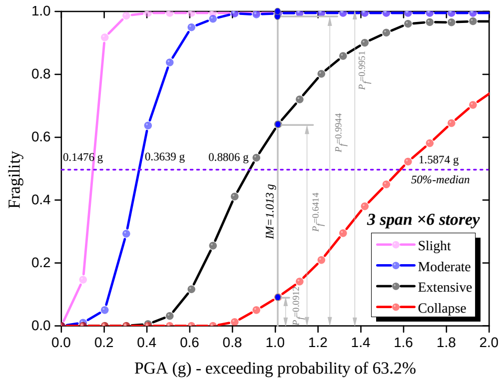

(a) Fragility with PGA exceeding probability of 63.2 %

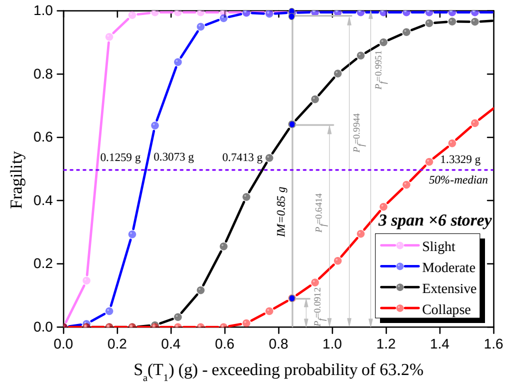

(b) Fragility with $S_a(T_1)$ exceeding probability of 63.2 %

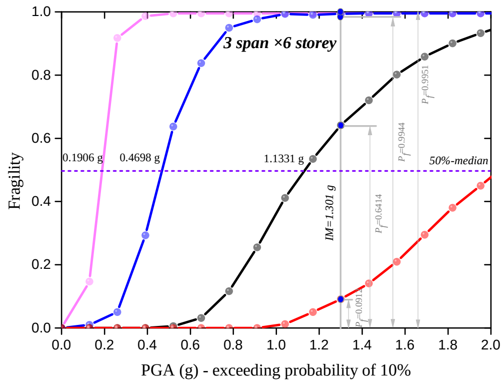

(c) Fragility with PGA exceeding probability of 10 %

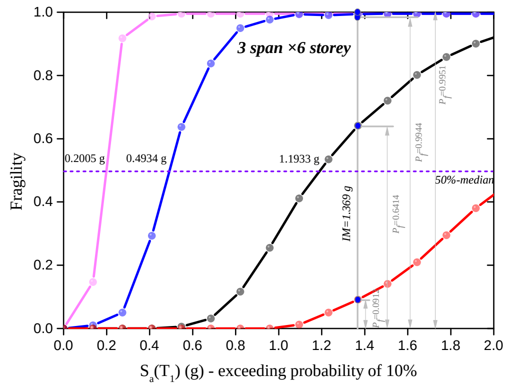

(d) Fragility with $S_a(T_1)$ exceeding probability of 10 %

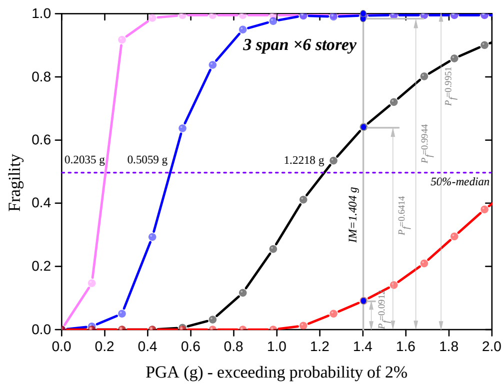

(e) Fragility with PGA exceeding probability of 2 %

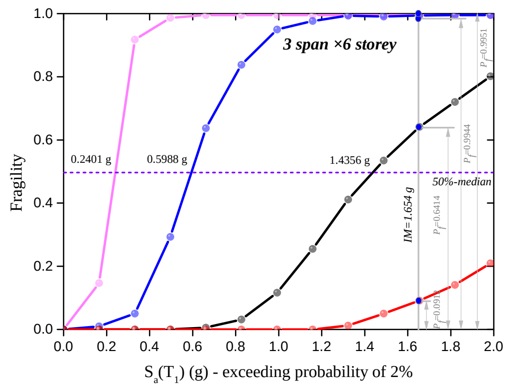

(f) Fragility with $S_a(T_1)$ exceeding probability of 2 %

Figure 11: The fragility curves with different exceeding probability of PGA or $S_a(T_1)$

a novel and accurate non-parametric PDEM-based approach for the consistent hazard-fragility analysis in the PBEE.

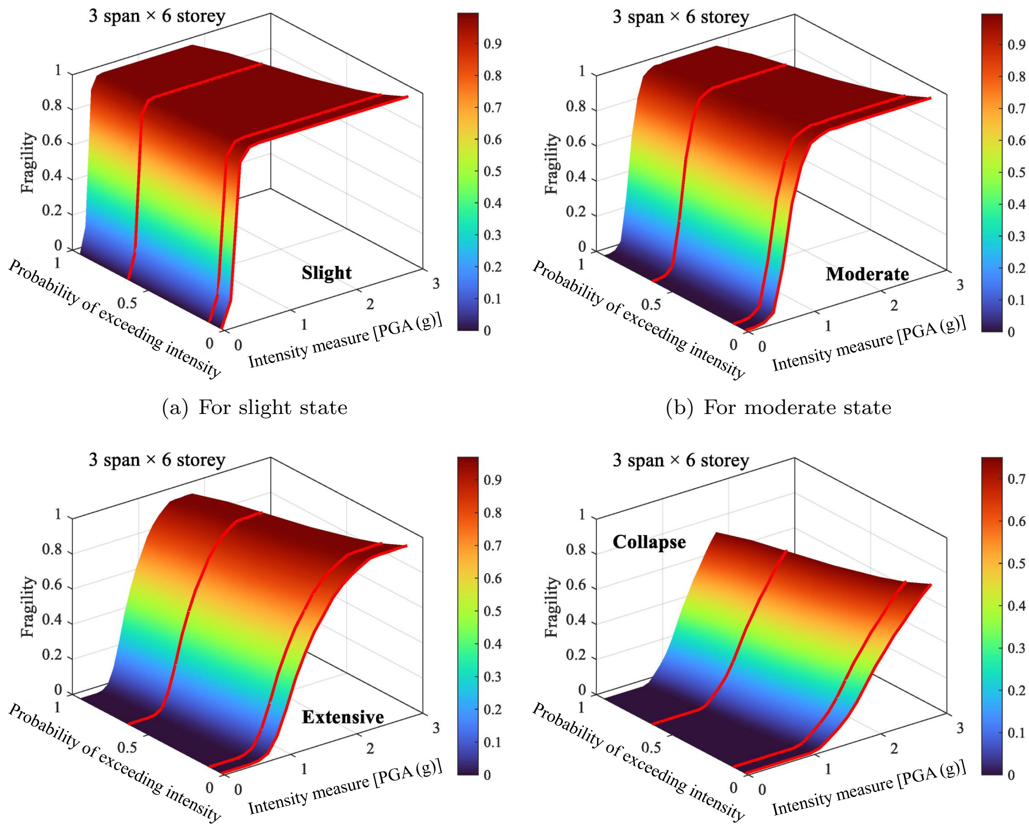

(a) For slight state

(b) For moderate state

(c) For extensive state

(d) For collapse state

Figure 12: Consistent 3D PDEM-based probabilistic hazard-fragility curves based on PGA

5.4. Comparison with the classic approaches in the state-of-the-art

To verify the accuracy of the proposed 3D consistent PDEM-based probabilistic curves, a comparison with the classic approaches in the state-of-the-art is performed in this subsection. The PDEM-based hazard curves are first compared with the theoretical hazard curves via both the PGA and $S_a(T_1)$, and the corresponding deviation coefficients are also calculated for analysis. Then, as the fragility result is the most important link in the full probabilistic framework and the critical connection in the proposed 3D consistent hazard-fragility expression, four classic fragility approaches are selected and well discussed, which are the linear regression method (LRM), maximum likelihood estimation (MLE), kernel density estimation (KDE), and Monte Carlo Simulation (MCS). Among the four selected approaches, the LRM and MLE are based on the parametric lognormal assumption, and the KDE and MCS are generated in light of the non-parametric theories without predefined shapes. The LRM is one of the most classic solutions, and in this analysis, it adopts the classic least-squares principle as well as the lognormal distribution. More details of the LRM equation can be found in Cornell et al. [1], Lallemant et al. [92], Bakalis and Vamvatsikos [94]. The MLE is under the lognormal assumption via a two-parameter-based equation (i.e., median value and logarithmic standard deviation), and its principle mainly lies in the differential calculation of the likelihood function. Shinozuka et al. [21] explained its theory detailedly, and more references of MLE are available in Baker [93] and Lelièvre et al [95]. The KDE is expressed in a pure non-parametric analytical form, and during the process, the marginal

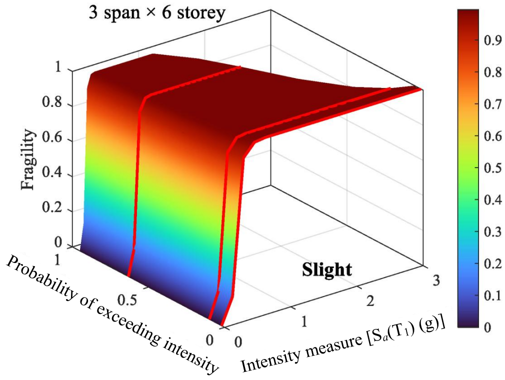

(a) For slight state

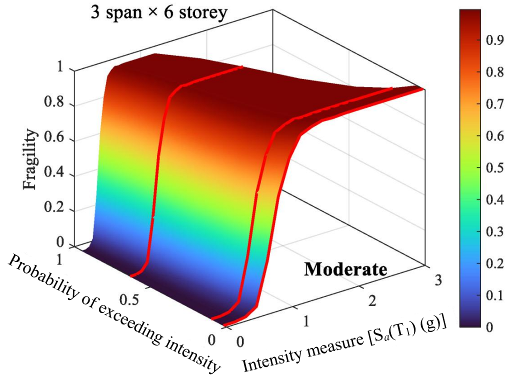

(b) For moderate state

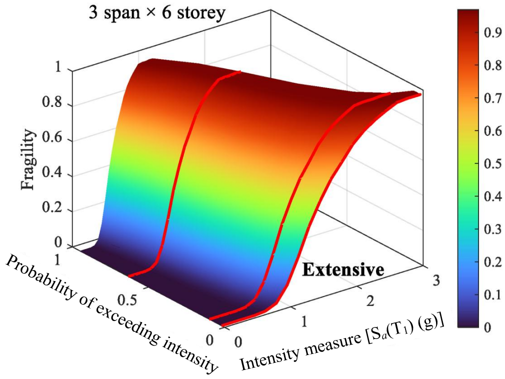

(c) For extensive state

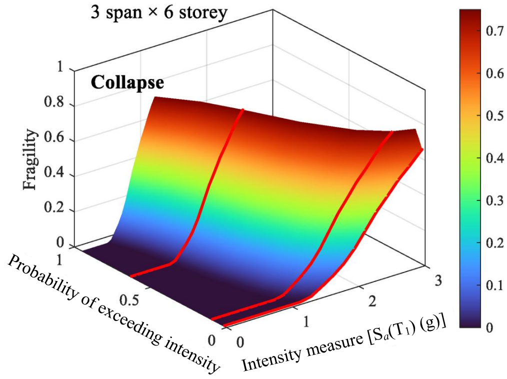

(d) For collapse state

Figure 13: Consistent 3D PDEM-based probabilistic hazard-fragility curves based on $S_a(T_1)$

PDF of intensity and the joint PDF between intensity-demand are both required. Sudret and Mai [88, 96] introduced its application into civil engineering, and more references of KDE can be found in Trevlopoulos et al. [97] and Lee [98]. As for the MCS, it is a commonly-used benchmark approach to evaluate the unknown statistical distributions and to verify the accuracy of a novel method by mass sampling. The approach is computationally consuming but can acquire the accurate results through sufficient data. More references of MCS are accessible in Echard et al. [99] and Naess et al [100]. In this analysis, the stochastic non-stationary earthquakes for LRM, MLE and KDE are in accordance with the inputs of PDEM (i.e., 200 samples for each earthquake level), and for MCS, 10000 sample sets are generated for each earthquake level as the benchmark.

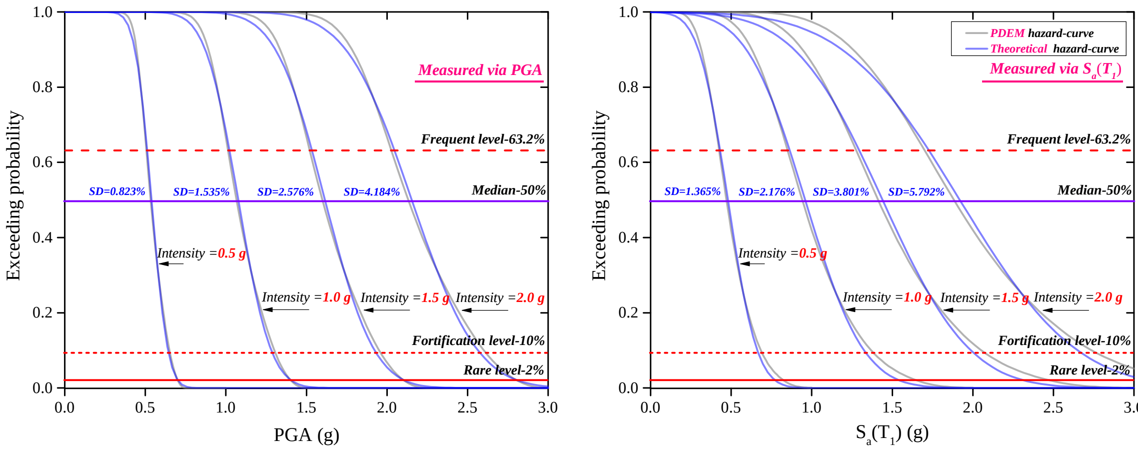

(a) Hazard comparison via the measure of PGA

(b) Hazard comparison via the measure of $S_a(T_1)$

Figure 14: Comparison between the PDEM-based and theoretical hazard curves

Fig. 14 displays the comparison between the PDEM-based and theoretical hazard curves for the 0.5 g, 1.0 g, 1.5 g, and 2.0 g levels, respectively. In general, good agreements can be observed between the two approaches. As for the intensity measure of PGA [Fig. 14(a)], the corresponding deviation coefficients for the four levels are calculated as 0.823 %, 1.535 %, 2.576 %, and 4.184 %, respectively, and for the intensity measure of $S_a(T_1)$ [Fig. 14(b)], the corresponding results for the four levels are given as 1.365 %, 2.176 %, 3.801 %, and 5.792 %, respectively. The average deviation is 2.782 %, indicating an ideal fitting degree between the two approaches in a sense. Besides, the PDEM-based hazard approach avoids the predefined shapes as well as the distribution types, and its corresponding assigned probability space can be directly connected to the subsequent fragility analysis to constitute a consistent hazard-fragility assessment. Fig. 15 to 18 display the LRM-based, KDE-based, MLE-based and MCS-based theories and application approaches for fragility, respectively. Both the static and dynamic results are integrated (i.e., CPI) for fragility assessment in this comparison study, and the PGA of non-stationary stochastic earthquake is adopted as the intensity measure for display in the following figures. To be specific, Fig. 15(a) and 15(b) reflect the lognormal fitting for capacity and least square regression for demand in the LRM, respectively. Fig. 16(a) and 16(b) reflect the marginal PDF of earthquake level and joint PDF between intensity-CPI in the KDE, respectively. Fig. 17(a) and 17(b) reflect the partial differential results of the two parameters in the lognormal equation in the MLE, respectively (via CPI). Fig. 18(a) to 18(d) display the scattered points for different limit states in the MCS, respectively (via CPI). For a clearer view, Fig. 19 presents the comparison with the classic approaches in the state-of-the-art (i.e., PDEM with the LRM, MLE, KDE and MCS), and the corresponding fitting coefficient (α) is summarized in Tab. 2. The expression of $\alpha = \sqrt{\sum_x^n (P_{f-app1-x} - P_{f-app2-x})^2/(n-1)}$, in which $P_{f-app1-x}$ and $P_{f-app2-x}$ denote the fragility of the approach 1 and approach 2 under the xth earthquake level, and n denotes the total intensity numbers. In general, it can be seen that the fragility tendency shows ideal consistency between the PDEM and MCS. For all the four limit states, the α-PDEM to the MCS is given as 0.0134, 0.0163, 0.0113 and 0.0107, which are all the smallest values in comparison with other approaches. As for the average α of PDEM (0.0129), its reducing ratios than the α-MLE (0.0316), α-LRM (0.0415) and α-KDE (0.0477) are calculated as 59.18 %, 68.92 % and 72.96 %, respectively, which indicates the accuracy of the PDEM-based fragility framework. Meanwhile, the computational efficiency of the PDEM-based method is significantly improved with less sample sets when compared with the benchmark MCS approach (i.e., 200 vs 10000), which demonstrates the superiority of the combined accuracy and efficiency of the non-parametric PDEM procedure, and further proves the applicability and fidelity of the 3D consistent non-parametric seismic hazard-fragility framework in a sense.

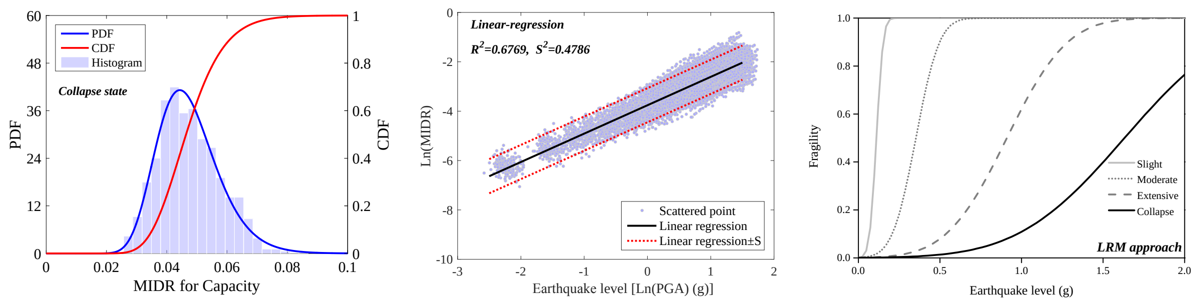

(a) Lognormal fitting for capacity (b) Least square regression for demand (c) LRM-based fragility

Figure 15: LRM-based theory and application approach for fragility

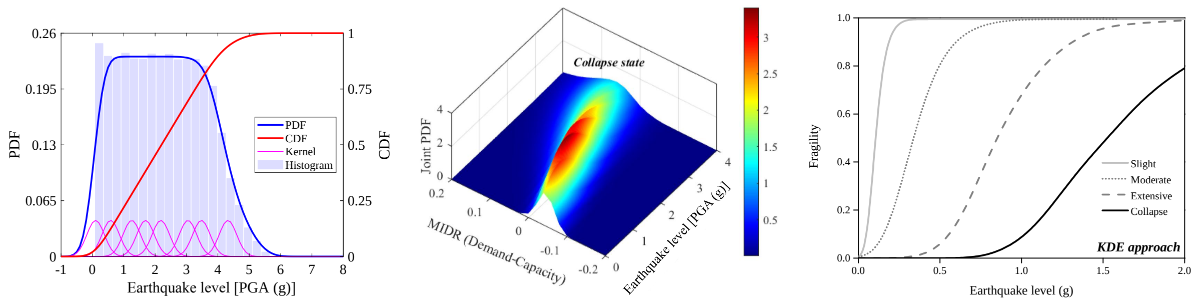

(a) Marginal PDF of earthquake level (b) Joint PDF between intensity and CPI (c) KDE-based fragility

Figure 16: KDE-based theory and application approach for fragility

Table 2: Comparison with the classic approaches in the state-of-the-art (PDEM with the LRM, MLE, KDE and MCS)

Number	***Limit state***	***α-MCS***	***α-PDEM***	***α-MLE***	***α-LRM***	***α-KDE***
1	Slight	benchmark (0)	0.0134	0.0335	0.0542	0.0713
2	Moderate	benchmark (0)	0.0163	0.0425	0.0427	0.0614
3	Extensive	benchmark (0)	0.0113	0.0205	0.0382	0.0301
4	Collapse	benchmark (0)	0.0107	0.0297	0.0307	0.0278
5	Average	benchmark (0)	0.0129	0.0316	0.0415	0.0477

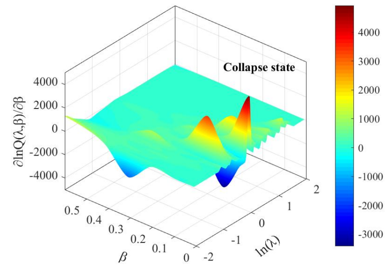

(a) $\frac{\partial lnQ(\lambda,\beta)}{\partial\lambda}$ in the two-parameter expression (via CPI)

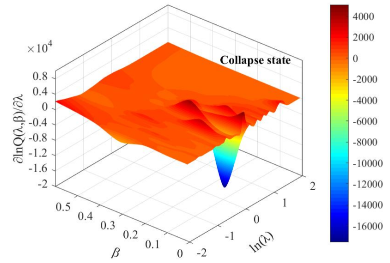

(b) $\frac{\partial lnQ(\lambda,\beta)}{\partial\beta}$ in the two-parameter expression (via CPI)

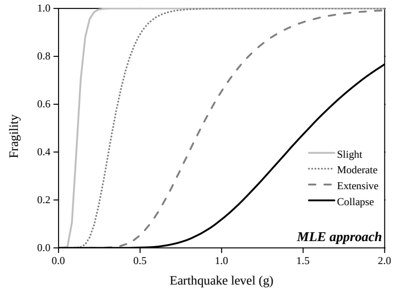

(c) MLE-based fragility

Figure 17: MLE-based theory and application approach for fragility

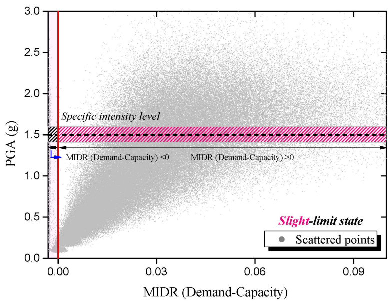

(a) MCS for slight state (via CPI)

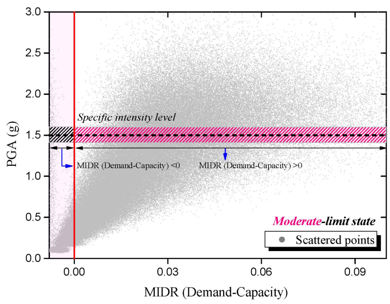

(b) MCS for moderate state (via CPI)

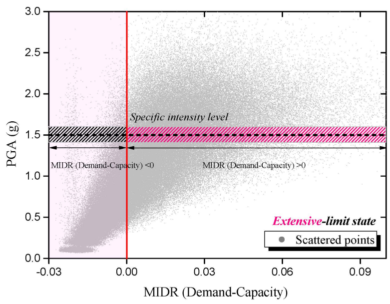

(c) MCS for extensive state (via CPI)

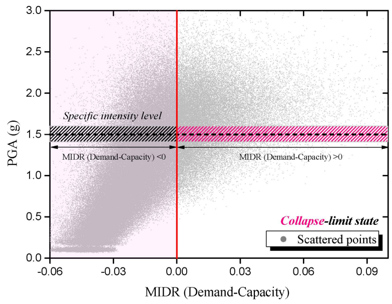

(d) MCS for collapse state (via CPI)

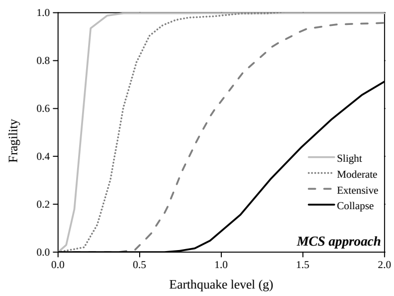

(e) MCS-based fragility

Figure 18: MCS-based theory and application approach for fragility

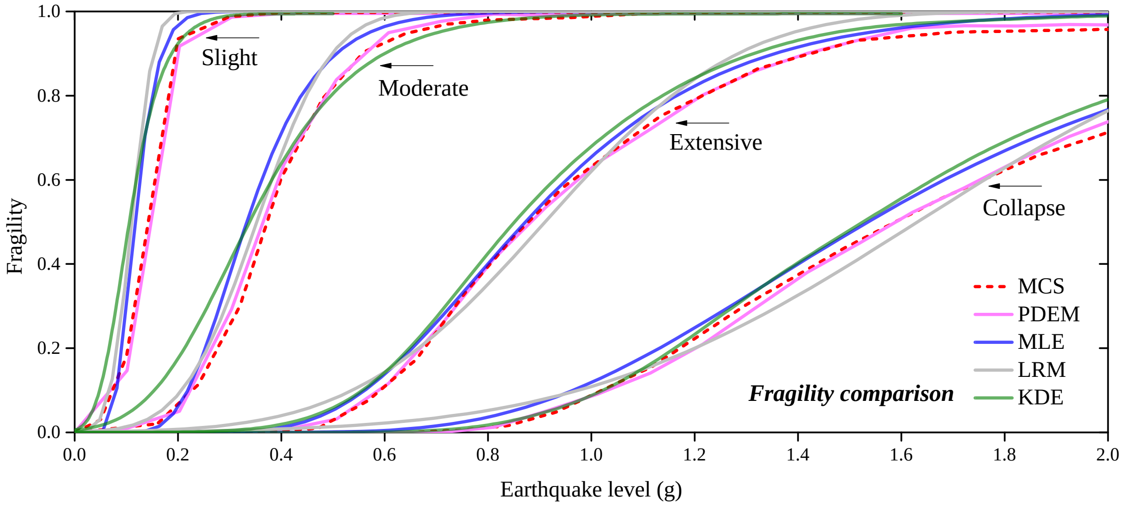

Figure 19: Comparison with the classic approaches in the state-of-the-art (PDEM with the LRM, MLE, KDE and MCS)

6. Conclusions

In this paper, a consistent seismic hazard and fragility framework with combined capacity-demand uncertainties is proposed. The well-known PDEM is applied, which has solid theoretical basis in the reliability field, and it is ideally integrated within the PBEE for hazard-fragility assessment. A non-stationary stochastic earthquake model is introduced, and the final 3D consistent hazard-fragility curves are given for predicting the structural performance considering multiple uncertainties. Different limit states, different earthquake levels as well as different intensity exceeding conditions can all be incorporated, and a comparison study with the classic approaches in the state-of-the-art (i.e., theoretical approach for hazard, LRM, MLE, KDE and MCS-based approaches for fragility) is performed to verify the accuracy of PDEM procedure, from which the following conclusions may be drawn:

As for the PDEM-based framework, the sample sets with different assigned probability are required to determine in advance through generalized F-Discrepancy method, which is a key step for the subsequent structural analysis and data summarization. The equivalent extreme events with virtual stochastic process are established during the process. Both the uncertainties of capacity and demand are considered, and a combined performance index (CPI) is defined as the concerned physical variable in PDEM, through pushover static and timehistory dynamic analyses. The information of earthquakes [e.g., PGA or $S_a(T_1)$] is also acquired as the concerned physical variable for each earthquake level, and then brought into the generalize PDEM equation for solution. The PDEM-based framework avoids the pre-defined lognormal curve shape and proves the combined efficiency and accuracy with the MCS.

As for the hazard-fragility analysis, the non-stationary stochastic ground motion is a key step in calculation, which is generated by spectral representation of random functions. The non-stationary stochastic ground motion avoids the limitations of natural ground motions and reflects more actual characteristics of ground motions by one or two variables. With the one or two variables, the earthquake model can be connected with the PDEM through each probability space and the statistical distributions of PGA or $S_a(T_1)$ for different earthquake levels can be constituted. The relationship between the fragility value and hazard extent is directly built without re-selecting ground motions, and the conditional probability in the full-probability formula can be directly satisfied. The probabilistic hazard-fragility analysis and the consistent 3D curves in this paper are mainly attributed to the application of PDEM and non-stationary earthquake models, which provides new ideas for the risk-based assessment scheme in the PBEE.

Acknowledgements

The first two authors greatly appreciate the Project of National Key Research and Development Program of China (Grant No. 2022YFC3803004), the National Natural Science Foundation of China (Grant Nos. 52208164 and 52078119), and the Natural Science Foundation of Jiangsu Province (Grant Nos. BK20220984 and BK20211564).

References

[1] C. A. Cornell, F. Jalayer, R. O. Hamburger, D. A. Foutch, Probabilistic basis for 2000 sac federal emergency management agency steel moment frame guidelines, Journal of structural engineering 128 (4) (2002) 526–533.

[2] O. C. Celik, B. R. Ellingwood, Seismic fragilities for non-ductile reinforced concrete frames–role of aleatoric and epistemic uncertainties, Structural Safety 32 (1) (2010) 1–12.

[3] X.-Y. Cao, D. Shen, D.-C. Feng, C.-L. Wang, Z. Qu, G. Wu, Seismic retrofitting of existing frame buildings through externally attached sub-structures: State of the art review and future perspectives, Journal of Building Engineering 57 (2022) 104904.

[4] S.-W. Han, Y.-S. Choi, Seismic hazard analysis in low and moderate seismic region-korean peninsula, Structural Safety 30 (6) (2008) 543–558.

[5] R. K. McGuire, Probabilistic seismic hazard analysis: Early history, Earthquake Engineering & Structural Dynamics 37 (3) (2008) 329–338.

[6] P. Tothong, C. A. Cornell, J. Baker, Explicit directivity-pulse inclusion in probabilistic seismic hazard analysis, Earthquake Spectra 23 (4) (2007) 867–891.

[7] I. Iervolino, M. Giorgio, B. Polidoro, Sequence-based probabilistic seismic hazard analysis, Bulletin of the Seismological Society of America 104 (2) (2014) 1006–1012.

[8] V. Convertito, A. Herrero, Influence of focal mechanism in probabilistic seismic hazard analysis, Bulletin of the Seismological Society of America 94 (6) (2004) 2124–2136.

[9] M. Z. Rahman, S. Siddiqua, A. M. Kamal, Seismic source modeling and probabilistic seismic hazard analysis for bangladesh, Natural Hazards 103 (2) (2020) 2489–2532.

[10] A. Q. Bhatti, S. Z. U. Hassan, Z. Rafi, Z. Khatoon, Q. Ali, Probabilistic seismic hazard analysis of islamabad, pakistan, Journal of Asian Earth Sciences 42 (3) (2011) 468–478.

[11] H. Ebrahimian, F. Jalayer, G. Forte, V. Convertito, V. Licata, A. dOnofrio, A. Santo, F. Silvestri, G. Manfredi, Site-specific probabilistic seismic hazard analysis for the western area of naples, italy, Bulletin of earthquake engineering 17 (9) (2019) 4743–4796.

[12] M. Mahsuli, H. Rahimi, A. Bakhshi, Probabilistic seismic hazard analysis of iran using reliability methods, Bulletin of Earthquake Engineering 17 (3) (2019) 1117–1143.

[13] M. W. Stirling, S. G. Wesnousky, K. R. Berryman, Probabilistic seismic hazard analysis of new zealand, New Zealand Journal of Geology and Geophysics 41 (4) (1998) 355–375.

[14] F. Jalayer, J. Beck, Effects of two alternative representations of ground-motion uncertainty on probabilistic seismic demand assessment of structures, Earthquake engineering & structural dynamics 37 (1) (2008) 61–79.

[15] S. Rezaeian, A. Der Kiureghian, Simulation of synthetic ground motions for specified earthquake and site characteristics, Earthquake Engineering & Structural Dynamics 39 (10) (2010) 1155–1180.

[16] I. Gidaris, A. A. Taflanidis, G. P. Mavroeidis, Kriging metamodeling in seismic risk assessment based on stochastic ground motion models, Earthquake Engineering & Structural Dynamics 44 (14) (2015) 2377–2399.

[17] X.-Y. Cao, D.-C. Feng, Y. Li, Assessment of various seismic fragility analysis approaches for structures excited by non-stationary stochastic ground motions, Mechanical Systems and Signal Processing 186 (2023) 109838.

[18] J.-W. Bai, P. Gardoni, M. B. D. Hueste, Story-specific demand models and seismic fragility estimates for multi-story buildings, Structural Safety 33 (1) (2011) 96–107.

[19] R. Gentile, C. Galasso, Gaussian process regression for seismic fragility assessment of building portfolios, Structural Safety 87 (2020) 101980.

[20] G. Lupoi, P. Franchin, A. Lupoi, P. E. Pinto, Seismic fragility analysis of structural systems, Journal of Engineering Mechanics 132 (4) (2006) 385–395.

[21] M. Shinozuka, M. Q. Feng, J. Lee, T. Naganuma, Statistical analysis of fragility curves, Journal of engineering mechanics 126 (12) (2000) 1224–1231.

[22] M. Schotanus, P. Franchin, A. Lupoi, P. Pinto, Seismic fragility analysis of 3d structures, Structural Safety 26 (4) (2004) 421–441.

[23] E. Choi, R. DesRoches, B. Nielson, Seismic fragility of typical bridges in moderate seismic zones, Engineering structures 26 (2) (2004) 187–199.

[24] D. H. Kim, S. G. Lee, I. K. Lee, Seismic fragility analysis of 5 mw offshore wind turbine, Renewable energy 65 (2014) 250–256.

[25] J. Park, P. Towashiraporn, J. I. Craig, B. J. Goodno, Seismic fragility analysis of low-rise unreinforced masonry structures, Engineering Structures 31 (1) (2009) 125–137.

[26] N. D. Lagaros, Y. Tsompanakis, P. N. Psarropoulos, E. C. Georgopoulos, Computationally efficient seismic fragility analysis of geostructures, Computers & Structures 87 (19-20) (2009) 1195–1203.

[27] M. A. Hariri-Ardebili, V. E. Saouma, Seismic fragility analysis of concrete dams: A state-of-the-art review, Engineering Structures 128 (2016) 374–399.
[28] X.-Y. Cao, D.-C. Feng, G. Wu, Z. Wang, Experimental and theoretical investigations of the existing reinforced concrete frames retrofitted with the novel external sc-pbspc brbf sub-structures, Engineering Structures 256 (2022) 113982.
[29] C.-L. Ning, Probabilistic seismic safety assessment based on probability density evolution theory (in chinese), Journal of Tongji University (natural science) 43 (3) (2015) 325–331.
[30] A. Karamlou, P. Bocchini, Computation of bridge seismic fragility by large-scale simulation for probabilistic resilience analysis, Earthquake Engineering & Structural Dynamics 44 (12) (2015) 1959–1978.
[31] S. Mangalathu, J.-S. Jeon, Stripe-based fragility analysis of multispan concrete bridge classes using machine learning techniques, Earthquake Engineering & Structural Dynamics 48 (11) (2019) 1238–1255.
[32] J. Li, J. Chen, The principle of preservation of probability and the generalized density evolution equation, Structural Safety 30 (1) (2008) 65–77.
[33] J. Li, J. Chen, W. Sun, Y. Peng, Advances of the probability density evolution method for nonlinear stochastic systems, Probabilistic Engineering Mechanics 28 (2012) 132–142.
[34] J. Chen, S. Yuan, Dimension reduction of the fpk equation via an equivalence of probability flux for additively excited systems, Journal of Engineering Mechanics 140 (11) (2014) 04014088.
[35] J. Chen, J. Yang, J. Li, A gf-discrepancy for point selection in stochastic seismic response analysis of structures with uncertain parameters, Structural Safety 59 (2016) 20–31.
[36] W. Fan, A. H.-S. Ang, Z. Li, Reliability assessment of deteriorating structures using bayesian updated probability density evolution method (pdem), Structural Safety 65 (2017) 60–73.
[37] Z. Wan, J. Chen, J. Li, A. H.-S. Ang, An efficient new pdem-com based approach for time-variant reliability assessment of structures with monotonically deteriorating materials, Structural Safety 82 (2020) 101878.
[38] T. Zhou, Y. Peng, Active learning and active subspace enhancement for pdem-based high-dimensional reliability analysis, Structural Safety 88 (2021) 102026.
[39] D.-C. Feng, X.-Y. Cao, M. Beer, An enhanced pdem-based framework for reliability analysis of structures considering multiple failure modes and limit states, Probabilistic Engineering Mechanics (2022) 103367.
[40] D. Patsialis, A. Taflanidis, Multi-fidelity monte carlo for seismic risk assessment applications, Structural Safety 93 (2021) 102129.
[41] Y. Bai, Y. Li, Z. Tang, M. Bittner, M. Broggi, M. Beer, Seismic collapse fragility of low-rise steel moment frames with mass irregularity based on shaking table test, Bulletin of Earthquake Engineering 19 (6) (2021) 2457–2482.
[42] X. Yu, Probabilistic seismic fragility and risk analysis of reinforced concrete frame structures, Ph.D thesis of Harbin Institute of Technology, China.
[43] F. Jalayer, P. Franchin, P. E. Pinto, A scalar damage measure for seismic reliability analysis of rc frames, Earthquake Engineering & Structural Dynamics 36 (13) (2007) 2059–2079.
[44] F. Jalayer, R. De Risi, G. Manfredi, Bayesian cloud analysis: efficient structural fragility assessment using linear regression, Bulletin of Earthquake Engineering 13 (4) (2015) 1183–1203.
[45] F. Jalayer, H. Ebrahimian, A. Miano, Intensity-based demand and capacity factor design: A visual format for safety checking, Earthquake Spectra 36 (4) (2020) 1952–1975.
[46] D. Vamvatsikos, C. Allin Cornell, Direct estimation of the seismic demand and capacity of oscillators with multi-linear static pushovers through ida, Earthquake engineering & structural dynamics 35 (9) (2006) 1097–1117.
[47] A. Surahman, Earthquake-resistant structural design through energy demand and capacity, Earthquake engineering & structural dynamics 36 (14) (2007) 2099–2117.
[48] E. Hernandez, M. Roohi, D. Rosowsky, Estimation of element-by-element demand-to-capacity ratios in instrumented smrf buildings using measured seismic response, Earthquake Engineering & Structural Dynamics 47 (12) (2018) 2561–2578.
[49] J. Li, J. B. Chen, J. Y. Yang, Pdem-based perspective to probabilistic seismic response analysis and design of earthquake-resistant engineering structures, Natural Hazards Review 18 (1) (2017) B4016002.
[50] W. Liu, Z. Li, Z. Song, J. Li, Seismic reliability evaluation of gas supply networks based on the probability density evolution method, Structural safety 70 (2018) 21–34.
[51] J. Xu, D.-C. Feng, Stochastic dynamic response analysis and reliability assessment of non-linear structures under fully non-stationary ground motions, Structural Safety 79 (2019) 94–106.
[52] D.-C. Feng, S.-C. Xie, Y. Li, L. Jin, Time-dependent reliability-based redundancy assessment of deteriorated rc structures against progressive collapse considering corrosion effect, Structural Safety 89 (2021) 102061.
[53] I. P. Mitseas, M. Beer, Fragility analysis of nonproportionally damped inelastic mdof structural systems exposed to stochastic seismic excitation, Computers & Structures 226 (2020) 106129.
[54] I. P. Mitseas, I. A. Kougioumtzoglou, A. Giaralis, M. Beer, A novel stochastic linearization framework for seismic demand estimation of hysteretic mdof systems subject to linear response spectra, Structural Safety 72 (2018) 84–98.
[55] G. Deodatis, Non-stationary stochastic vector processes: seismic ground motion applications, Probabilistic engineering mechanics 11 (3) (1996) 149–167.
[56] P. Cacciola, G. Deodatis, A method for generating fully non-stationary and spectrum-compatible ground motion vector processes, Soil Dynamics and Earthquake Engineering 31 (3) (2011) 351–360.
[57] J. Ou, G. Wang, Random vibration of structures (in Chinese), Higher Education Press, 1998.
[58] Z. Liu, B. Zeng, L. Wu, Spectral representation of non-stationary ground motion process simulation: Random function method (in chinese), Journal of Vibration Engineering 28 (3) (2015) 411–417.
[59] M. Shinozuka, G. Deodatis, Simulation of stochastic processes by spectral representation.
[60] M. Shinozuka, G. Deodatis, Simulation of multi-dimensional gaussian stochastic fields by spectral representation.

[61] Z. Liu, W. Liu, Y. Peng, Random function based spectral representation of stationary and non-stationary stochastic processes, Probabilistic Engineering Mechanics 45 (2016) 115–126.
[62] R. Pang, Y. Zhou, G. Chen, M. Jing, D. Yang, Stochastic mainshock–aftershock simulation and its applications in dynamic reliability of structural systems via dpim, Journal of Engineering Mechanics 149 (1) (2023) 04022096.
[63] ASCE (American Society of Civil Engineering). (2010). Minimum Design Loads for Buildings and Other Structures (ASCE/SEI 7-10), Reston, VA.
[64] S. Mazzoni, F. McKenna, M. H. Scott, G. L. Fenves, et al., Opensees command language manual, Pacific Earthquake Engineering Research (PEER) Center, Berkeley, CA.
[65] F. McKenna, G. L. Fenves, M. H. Scott, et al., Open system for earthquake engineering simulation, University of California, Berkeley, CA.
[66] D.-C. Feng, Z. Wang, X.-Y. Cao, G. Wu, Damage mechanics-based modeling approaches for cyclic analysis of precast concrete structures: A comparative study, International Journal of Damage Mechanics 29 (6) (2020) 965–987.
[67] X.-Y. Cao, G. Wu, J.-W. W. Ju, Seismic performance improvement of existing rcfs using external pt-pbspc frame substructures: Experimental verification and numerical investigation, Journal of Building Engineering 46 (2022) 103649.
[68] J. B. Mander, M. J. Priestley, R. Park, Theoretical stress-strain model for confined concrete, Journal of structural engineering 114 (8) (1988) 1804–1826.
[69] B. D. Scott, R. Park, M. J. N. Priestley, Stress-strain behavior of concrete confined by overlapping hoops at low and high strain rates, ACI Journal 79 (1) (1982) 13–27.
[70] X.-Y. Cao, G. Wu, D.-C. Feng, Z. Wang, H.-R. Cui, Research on the seismic retrofitting performance of rc frames using sc-pbspc brbf substructures, Earthquake Engineering & Structural Dynamics 49 (8) (2020) 794–816.
[71] F. J. Vecchio, M. P. Collins, The modified compression-field theory for reinforced concrete elements subjected to shear, ACI Journal 83 (2) (1986) 219–231.
[72] X.-Y. Cao, C.-Z. Xiong, D.-C. Feng, G. Wu, Dynamic and probabilistic seismic performance assessment of precast prestressed reinforced concrete frames incorporating slab influence through three-dimensional spatial model, Bulletin of Earthquake Engineering (2022) 1–35.
[73] T.-S. Eom, H.-G. Park, H.-J. Hwang, S.-M. Kang, Plastic hinge relocation methods for emulative pc beam–column connections, Journal of Structural Engineering 142 (2) (2016) 04015111.
[74] MHURD-PRC (Ministry of Housing and Urban-Rural Development of the People's Republic of China).(2010). Code for design of concrete structures (GB50010), Beijing (in Chinese).
[75] X.-Y. Cao, D.-C. Feng, G. Wu, Pushover-based probabilistic seismic capacity assessment of rcfs retrofitted with pbspc brbf sub-structures, Engineering Structures 234 (2021) 111919.
[76] X.-Y. Cao, D.-C. Feng, G. Wu, J.-G. Xu, Probabilistic seismic performance assessment of rc frames retrofitted with external sc-pbspc brbf sub-structures, Journal of Earthquake Engineering (2021) 1–24.
[77] FEMA (Federal Emergency Management Agency). (2003). Multi-hazard loss estimation methodology, earthquake model, Washington, DC.
[78] FEMA (Federal Emergency Management Agency). (2012). Seismic Performance Assessment of Buildings Volume 1-Methodology (FEMA P-58-1), Washington, DC.
[79] R. Villaverde, Methods to assess the seismic collapse capacity of building structures: State of the art, Journal of Structural Engineering 133 (1) (2007) 57–66.
[80] A. Kazantzi, D. Vamvatsikos, D. Lignos, Seismic performance of a steel moment-resisting frame subject to strength and ductility uncertainty, Engineering Structures 78 (2014) 69–77.
[81] F. Freddi, J. E. Padgett, A. DallAsta, Probabilistic seismic demand modeling of local level response parameters of an rc frame, Bulletin of Earthquake Engineering 15 (1) (2017) 1–23.
[82] J. Xu, D.-C. Feng, Seismic response analysis of nonlinear structures with uncertain parameters under stochastic ground motions, Soil Dynamics and Earthquake Engineering 111 (2018) 149–159.
[83] CABR (China Academy of Building Research).(1984). Unified standards for building structure design (GBJ68-84), Beijing (in Chinese).
[84] D.-C. Feng, S.-C. Xie, J. Xu, K. Qian, Robustness quantification of reinforced concrete structures subjected to progressive collapse via the probability density evolution method, Engineering Structures 202 (2020) 109877.
[85] M. Barbato, Q. Gu, J. Conte, Probabilistic push-over analysis of structural and soil-structure systems, Journal of structural engineering 136 (11) (2010) 1330–1341.
[86] J. Li, J.-B. Chen, The probability density evolution method for dynamic response analysis of non-linear stochastic structures, International Journal for Numerical Methods in Engineering 65 (6) (2006) 882–903.
[87] J.-B. Chen, J. Li, The extreme value distribution and dynamic reliability analysis of nonlinear structures with uncertain parameters, Structural Safety 29 (2) (2007) 77–93.
[88] C. Mai, K. Konakli, B. Sudret, Seismic fragility curves for structures using non-parametric representations, Frontiers of Structural and Civil Engineering 11 (2) (2017) 169–186.
[89] D. Altieri, E. Patelli, An efficient approach for computing analytical non-parametric fragility curves, Structural Safety 85 (2020) 101956.
[90] R. Kennedy, M. Ravindra, Seismic fragilities for nuclear power plant risk studies, Nuclear engineering and design 79 (1) (1984) 47–68.
[91] F. Jalayer, C. Cornell, Alternative non-linear demand estimation methods for probability-based seismic assessments, Earthquake Engineering & Structural Dynamics 38 (8) (2009) 951–972.
[92] D. Lallemant, A. Kiremidjian, H. Burton, Statistical procedures for developing earthquake damage fragility curves, Earthquake Engineering & Structural Dynamics 44 (9) (2015) 1373–1389.

[93] J. W. Baker, Efficient analytical fragility function fitting using dynamic structural analysis, Earthquake Spectra 31 (1) (2015) 579–599.
[94] K. Bakalis, D. Vamvatsikos, Seismic fragility functions via nonlinear response history analysis, Journal of structural engineering 144 (10) (2018) 04018181.
[95] N. Lelièvre, P. Beaurepaire, C. Mattrand, N. Gayton, Ak-mcsi: A kriging-based method to deal with small failure probabilities and time-consuming models, Structural Safety 73 (2018) 1–11.
[96] B. Sudret, C. Mai, K. Konakli, Assessment of the lognormality assumption of seismic fragility curves using non-parametric representations, arXiv preprint arXiv:1403.5481.
[97] K. Trevlopoulos, C. Feau, I. Zentner, Parametric models averaging for optimized non-parametric fragility curve estimation based on intensity measure data clustering, Structural Safety 81 (2019) 101865.
[98] S. Lee, Monte carlo simulation using support vector machine and kernel density for failure probability estimation, Reliability Engineering & System Safety 209 (2021) 107481.
[99] B. Echard, N. Gayton, M. Lemaire, Ak-mcs: an active learning reliability method combining kriging and monte carlo simulation, Structural Safety 33 (2) (2011) 145–154.
[100] A. Naess, B. Leira, O. Batsevych, System reliability analysis by enhanced monte carlo simulation, Structural safety 31 (5) (2009) 349–355.